Organic & Biomolecular Chemistry

Radical Enhanced Intersystem Crossing Mechanism, Electron Spin Dynamics of High Spin States and Applications in Design of Heavy Atom-free Triplet Photosensitizers

Journal:	*Organic & Biomolecular Chemistry*
Manuscript ID	OB-REV-03-2024-000520.R1
Article Type:	Review Article
Date Submitted by the Author:	21-May-2024
Complete List of Authors:	Zhang, Xue; Dalian University of Technology, State Key Laboratory of Fine Chemicals Chen, Xi; Dalian University of Technology, State Key Laboratory of Fine Chemicals Sun, Yue; Dalian University of Technology, Zhao, Jianzhang; Dalian University of Technology, State Key Laboratory of Fine Chemicals;

REVIEW

Radical Enhanced Intersystem Crossing Mechanism, Electron Spin Dynamics of High Spin States and Applications in Design of Heavy Atom-free Triplet Photosensitizers

Received 00th January 20xx,
Accepted 00th January 20xx

DOI: 10.1039/x0xx00000x

Xue Zhang,*[a] Xi Chen,[a] Yue Sun[a] and Jianzhang Zhao*[a]

Heavy atom-free triplet photosensitizers (PSs) can overcome the high cost and biological toxicity of traditional molecular systems contain heavy atoms (such as Pt(II), Ir(III), Ru(II), Pd(II), Lu(III) or I, Br atoms), therefore are developing rapidly these years. Connecting the stable free radical to the chromophore can promote the intersystem crossing (ISC) process through electron spin exchange interaction to produce the triplet state, or the doublet (D) and quartet (Q) states by taking the whole spin system into account. These molecular systems based on radical enhanced ISC (REISC) mechanism are important in the field of heavy atom-free triplet PSs. REISC system has simple molecular structure and good biocompatibility, especially it is helpful to build high-spin quantum states (D and Q states), which have the potential to be developed as the qubit in quantum information science. This review introduced the molecular structure design for the purpose of high-spin states. Time-resolved electron paramagnetic resonance (TREPR) is the most important characterization method to reveal the properties, generation mechanism and electron spin polarization (ESP) of the high spin states. The spin polarization manipulation of high spin states and the potential application in the field of quantum information engineering are also summarized. Moreover, the molecular design principle of REISC system to obtain long absorption wavelength, high triplet state quantum yield and long triplet state lifetime are introduced, as well as the applications of the compounds in triplet-triplet annihilation upconversion, photodynamic therapy and bioimaging. This review article is useful to design heavy atom-free triplet PSs based on radical-chromophore molecular structure motif, and study the photophysics of the compounds, as well as the electron spin dynamics of the multi electron system upon photoexcitation.

1. Introduction

Triplet photosensitizers (PSs) are compounds showing strong absorption ability, efficient intersystem crossing (ISC), appropriate redox potentials, and robust stability. They are widely used in photovoltaic materials,[1–3] artificial photosynthesis,[4–6] photodynamic therapy (PDT)[7–9] and photon upconversion,[10–12] etc. ISC process accompanied by spin multiplicity changes, which is an electron spin-forbidden transition, only very few molecules can be directly photoexcited to the triplet states,[13,14] most triplet PSs through ISC to generate T_n states from singlet excited states (usually from S_1 state, Kasha's rule). One of traditional methods to generate triplet

[a] State Key Laboratory of Fine Chemicals, Frontiers Science Centre for Smart Materials, School of Chemical Engineering, Dalian University of Technology, Dalian 116024, P. R. China. E-mail: zhangxue@dlut.edu.cn (X. Z.) and zhaojzh@dlut.edu.cn (J. Z.)

Dr. Xue Zhang obtained her PhD degree in School of Chemical Engineering from Dalian University of Technology in 2023. She is now a postdoctoral research fellow in Prof. Jianzhang Zhao's group. Her research interests mainly focus on the synthesis and spectroscopic characterization of heavy-atom free triplet photosensitizers with steady state, femtosecond/nanosecond transient absorption spectroscopies and time-resolved electron paramagnetic resonance (TREPR) spectroscopy.

Xi Chen received her B.S. and M.S. degrees in applied chemistry from Dalian University of Technology in 2018 and 2021, respectively. Since 2021, she has been a PhD student in Prof. J. Zhao's group. Her research focuses on the synthesis of heavy atom-free triplet photosensitizers and the study of intersystem crossing and charge separation processes using steady state and time-resolved transient spectroscopy.

state is via introducing atoms with large atomic mass into the chromophore, such as Pt(II), Ir(III), Ru(II), Pd(II), Lu(III) transition metal complexes[15–18] or compounds contain I or Br atoms.[19,20] However, the participation of the heavy atom in the molecular orbital electron wavefunction distribution is required for heavy atom effect (El Sayed rule).[21] It should be noted that the spin-orbital coupling (SOC) can promote ISC to produce triplet states ($S_1 \rightarrow T_n$), it can also promote the ISC process $T_1 \rightarrow S_0$ to a certain extent, this effect may shorten the excited triplet state lifetime, which is detrimental to the application of the triplet PSs, in addition, the high cost and biological toxicity of heavy atoms also limit their applications. Therefore, the development of heavy atom-free triplet PS is necessary.

Recently, a few mechanisms to achieve ISC in heavy atom-free triplet systems have been developed. Charge recombination (CR) induced ISC has been known for a long time, however, it was usually observed in compounds with complicated molecular structure, and they are not designed for attaining efficient population of the locally excited (LE) state (i.e. the triplet state is confined on a single chromophore in the molecular structure). This method is beneficial to obtain long lived triplet excited state recently.[22,23] The systems are mainly composed by two parts: electron donor and acceptor (some systems also include the bridge groups, i.e. the linkers between the donor and acceptor), the molecules can be excited to the locally excited singlet state (^{1}LE) of the donor or acceptor, the redox ability of the ^{1}LE state is enhanced in comparison with the S_0 state, the charge separation (CS) with singlet precursor (e.g. ^{1}LE) is more likely to result in the CS singlet excited state (^{1}CS). Due to the electron spin conservation rule, the ^{1}CS $\rightarrow$ ^{3}CS ISC is quenched by the large *J* value. However, If the distance between the donor and acceptor is long, the electron exchange interaction between donor and acceptor is weak enough (the electron exchange energy *J* value is small), the energy difference between the ^{1}CS and the ^{3}CS states is very small (e.g. $\Delta E_{ST} = 2J < 0.1$ cm^{-1}), the hyperfine coupling interaction (HFI, interaction between unpaired electron spin magnetic moment and nuclear spin magnetic moment) can promote the ISC of ^{1}CS $\rightarrow$ ^{3}CS, the process is called radical pair ISC (RP-ISC).[24,25] Subsequently, the ^{3}CS state deactivate to the S_0 state, or to ^{3}LE state, given the ^{3}LE energy is lower than CS state via CR process of ^{3}CS $\rightarrow$ ^{3}LE (internal conversion process).[24,26] Molecules based on the RP-ISC mechanism usually require long and rigid bridge groups between donor and acceptor,[27,28] which makes the synthesis of the compounds challenging. What's more, the slow ISC induced by HFI (time scale is at nanoseconds) is not helpful to generate high triplet state quantum yield (Φ_T).[24,29,30] In contrast, the compact donor-acceptor dyad molecular structure motifs have become promising to attain efficient ISC. In the molecular structure of these compounds, the electron donor and acceptor are directly connected through a single bond, forming a near-vertical conformation for the π–conjugation planes of the donor and acceptor.[31–33] In this case, the electronic coupling between donor and acceptor is relatively strong, and the *J* value is increased (the energy level difference between ^{1}CS and ^{3}CS states is larger than the dyads containing long linker), HFI is not sufficient to promote the ISC process of ^{1}CS $\rightarrow$ ^{3}CS, however, the CR of ^{1}CS state can directly generate ^{3}LE state (^{1}CS $\rightarrow$ ^{3}LE), which is called the spin-orbital charge transfer ISC (SOCT-ISC) process.[21,23,34] During the ISC process, the change of molecular orbital angular momentum (the π–conjugation framework of the electron donor and acceptor are not in the same plane) compensates for the change of electron spin angular momentum during ISC process and complies with the conservation of total angular momentum. Our group reported a series of SOCT-ISC systems and studied the molecular structure-efficiency relationship, for example, the systems based on naphthaldiimide (NDI),[35,36] perylenebisimide (PBI),[37,38] Bodipy,[39,40] etc, were studied. It should be noted that when the energy level of ^{3}LE state is slightly lower than ^{1}CT state, the SOCT-ISC will produce ^{3}LE effectively. If the energy level of ^{1}CT

Yue Sun received her B.S. degree in applied chemistry from Dalian University of Technology. She proceed a M.S. degree at Dalian University of Technology in 2021. Since 2023, she has been a PhD student in Prof. J. Zhao's group. Her research mainly focuses on synthesis of triplet photosensitizers showing long lifetime, and study the photophysical property using steady-state spectroscopy and time-resolved transient spectroscopy.

Prof. Jianzhang Zhao received his PhD degree in organic chemistry from Jilin University. After postdoctoral research at the Pohang University of Science and Technology (POSTECH South Korea), the Max Planck Research Unit for Enzymology of Protein Folding (Halle, Germany) and the University of Bath (U. K.), he took his current position at Dalian University of Technology. His research interests include synthesis of triplet photosensitizers, and study of the intersystem crossing, electron transfer and electron spin dynamics of the compounds upon photoexcitation with steady-state and femtosecond/nanosecond transient absorption spectroscopies, as well as pulsed laser excited time-resolved electron paramagnetic resonance (TREPR) spectroscopy.

state is lower than that of ^{3}LE state, CR from ^{1}CT to the ground state will be dominant.

The CS states have relatively large dipole moment, the energy level are sensitive to the solvent polarity, the strength of electron coupling and other relevant factors (the LE state has a smaller dipole moment, so its energy level is little affected by the above factors). When the ^{1}CS and ^{3}LE states energy are close to each other (the energy level difference is close to the room temperature thermal energy of 26 meV), the energy can be effectively converted from ^{3}LE to ^{1}CS state by a reverse ISC (RISC) process driven by thermal activation, the ^{1}CS state emits thermally activated delayed fluorescence (TADF). In other words, TADF molecules which are widely used in the organic light-emitting diode field, are the special case of SOCT-ISC systems. The overlap of HOMO and LUMO of these molecules is small, therefore the ΔE between ^{1}CS and ^{3}CS is also small. In such systems, the three-states model is proposed recently, i.e. the ^{1}CT, ^{3}LE and ^{3}CT states are close to each other in energy, and the spin-vibronic coupling between ^{3}LE and ^{3}CT promotes the RISC. Our group has used transient absorption spectra and time-resolved electron paramagnetic resonance (TREPR) spectral methods to experimentally confirm this model.[35,41–44]

Another mechanism to promote ISC is based on distorted molecular structures, it is proposed that the small spatial overlap of the molecular orbitals resulted in a small J value (small $\Delta E_{ST} = 2J$) and large spin orbit coupling matrix elements (SOCMEs).[21,45] The ISC efficiency of Fullerene C_{60} is close to 100% due to the highly distorted π–conjugated structure, however, the absorption of C_{60} in the visible light region is very weak, and the poor solubility limited the application of C_{60} as an ideal triplet PS.[46] Helicene is another representative compounds having twisted π–conjugated framework and exhibits high ISC efficiency, and it was found that the ISC efficiency is proportional to the twisting extent of the π–conjugation system.[45] However, the synthesis and derivatization of helicene are difficult, and the absorption wavelength is short, generally located in the ultraviolet region, therefore, most of the traditional helicenes are not ideal triplet PSs. In recent years, researchers have extended the structure motif to PBI and Bodipy chromophores. For example, Hariharan's group reported twisted PBI derivatives, proved that the Herzberg-Teller vibronic coupling promote the ISC process, and the ISC quantum yields were determined as Φ_T of 63% and 23%, respectively.[47] Our group studied Bodipy derivative with twisted molecular structure, and the ISC quantum yield was determined as Φ_T of 52%, and the intrinsic triplet lifetime is 492 μs, which has been used in PDT successfully.[48] However, it is still in doubt whether or not the twisting of the molecular structure will always induce ISC ability. Recently, it is found that in some molecular structures, the twisted angle may be not correlated with the ISC efficiency, a minor distortion can also result in a high ISC efficiency, on the contrary, a large torsion angle is unnecessary to induce high ISC ability.[49,50] This is a solid evidence that there is no simple correlation between the twisting of the molecular structure and the ISC ability, and those compounds with twisted molecular structure showing ISC, are probably merely by coincidence. The underlying principle is probably the S_m and T_n states energy matched, however, it is necessary to further exploit the relationship between the twisted molecular structure and the ISC ability.

In contrast to the above mechanisms, radical enhanced ISC (REISC) mechanism can transform the spin-forbidden ISC process into the spin-allowed internal conversion process directly, thereby enhancing the generation of triplet states. These systems are based on introducing the stable free radicals into organic chromophore and enhancing ISC by electron spin-spin exchange interaction (Fig. 1). The radical and chromophore form three-electron spin system, the total spin multiple of the system can be two (doublet states, D) or four (quartet states, Q).[51–53] When the singlet electron configuration chromophore undergoes spin exchange interaction with radical single electrons, the total spin multiplicity of the system is two (^{2}[S_1, R], D_2). When the chromophore is in the triplet electron configuration, the total spin multiplicity of the system can be two (^{2}[T_1, R], D_1) or four (^{4}[T_1, R], Q_1).[52] The ISC process for ^{2}[S_1, R] → ^{2}[T_1, R] is spin-allowed, which can enhance the population of triplet states of chromophore (D_1 state), with the zero field splitting (ZFS) or other effect, the Q_1 state can also generated (we use D_0 stand for ^{2}[S_0, R], D_2 stand for ^{2}[S_1, R], D_1 stand for ^{2}[T_1, R] and Q stand for ^{4}[T_1, R] in the discussion of this review).

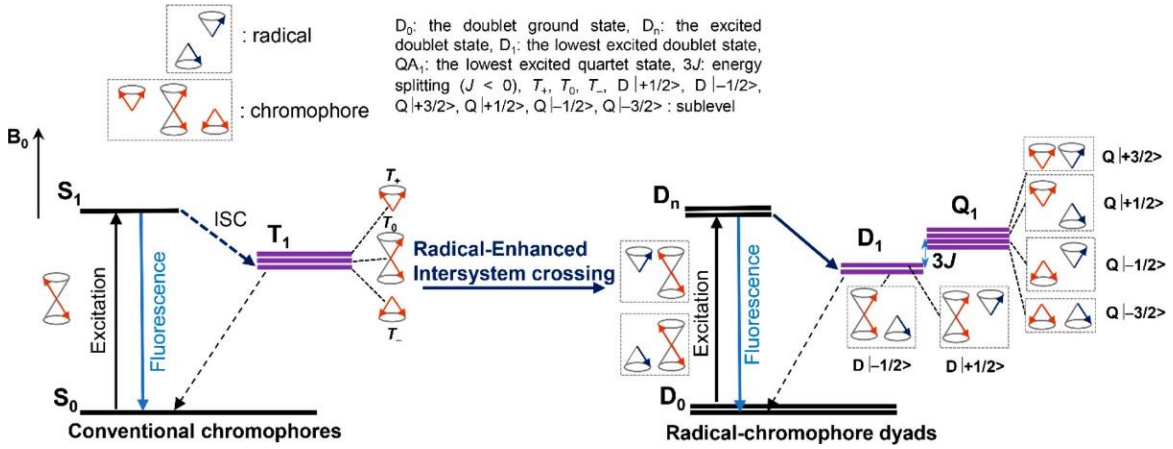

Fig. 1 Simplified energy diagrams of conventional chromophores based on SOC-ISC and novel chromophores based on REISC mechanisms. Reproduced with permission from ref. 9. Copyright 2021 American Chemical Society.

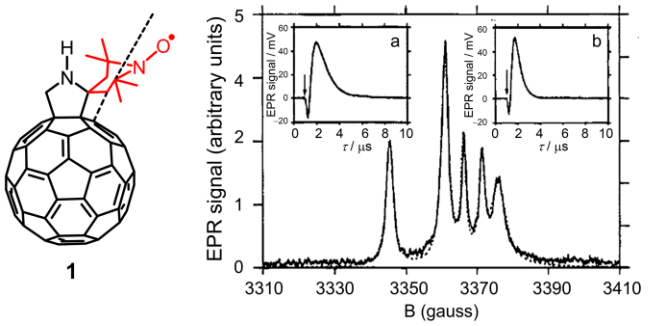

Fig. 2 The molecular structure of C_{60}-nitroxide radical molecule **1** and TREPR spectra at 200 K, insets show the time volution of the EPR signal at (a) 3346 G and (b) 3366 G. Reproduced with permission from ref. 73. Copyright 1995 American Chemical Society.

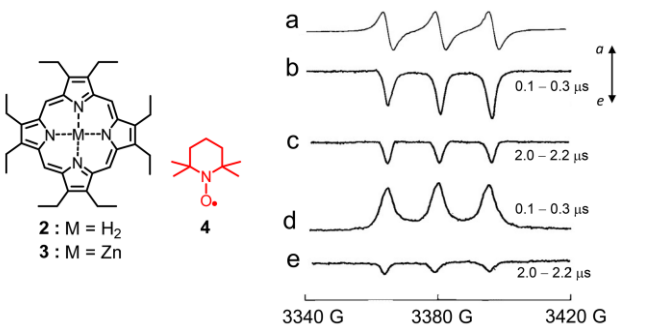

Fig. 3 The molecular structures of porphyrin and nitroxide radical systems and (a) steady-state EPR spectrum of TEMPO **4** and TREPR spectra of the (b, c) **2** and (d, e) **3** at different decay time. Reproduced with permission from ref. 74. Copyright 1997 American Chemical Society.

The molecular system undergoes REISC is simple and easy to synthesize, even without orbital overlap can also enhanced ISC, it is expected to be a new strategy for the development of heavy atom-free triplet photosensitizers. Moreover, the photoexcitation generated high spin states are useful in quantum information science, for instance, the radical-chromophore molecular system can be used for development of molecular qubits or qudits.[54–58]

The ISC of organic compounds is electron spin selective, i.e. the population of the three sublevels of T_x, T_y and T_z of the T_1 state is severely deviated from the Boltzman distribution, this is caused by the anisotropic SOC effect. The electron spin polarization (ESP) is also an important property in REISC system, there are two main mechanisms of ESP: radical-triplet pair mechanism (RTPM)[59–61] and electron spin polarization transfer (ESPT) mechanism.[62,63] In the RTPM, the triplet states and radicals are diffused with each other in solution, and the spin states are mixed by spin exchange interaction to produce a spin polarized D_1 and Q_1 states, this effect is dependent on the distance between the two species. The ESPT mechanism requires the formation of a polarized triplet excited state precursor, followed by the transfer of ESP to the D_0 state of the free radical.[64] For REISC systems, the spin interactions between radicals and chromophores are complex, the structure-efficiency relationship of molecules is not very clear. Therefore, it needs to be further studied and the diversity of the chromophore need to be extended. This review article introduced the characterization methods of high spin states and the ESP characteristics of different REISC mechanisms in detail, also summarized the molecular structure design principles of triplet photosensitizers based on REISC mechanism. It also introduced the potential applications of REISC system as qubits or qudits,[26,65–67] and made an outlook of REISC mechanism in bioimaging,[68,69] triplet-triplet annihilation up-conversion (TTA-UC),[70] PDT,[71,72] etc. This review article will facilitate ultimately possibility to establish design protocols for exhibiting the desired properties for triplet PSs based on ERISC mechanism. It should be pointed out that some molecules contain multiple radicals, which can build more complex spin systems and produce higher spin states, such as quintuplet states. Moreover, the transient pulse EPR spectroscopy is also an important method to study the high spin states and the mechanism. With different EPR pulse sequences applied, the nutation frequency and relaxation time can be obtained. These contents are already covered in the previous review,[26] they are not introduced in this review.

2. Observation and mechanisms study of high spin states generated by REISC

The REISC mechanism with the electron spin exchange interaction produce the high spin D and Q states cannot be distinguished by the transient absorption optical spectra (in both states, the electronic configurations of chromophore are always in open shell), because the difference of these two excited states is only reflected in the electron spin-spin interaction between the radical and the triplet state, there is no any difference of molecular orbital occupancy. TREPR spectroscopy can characterize the ESP of the photogenerated transient paramagnetic species, which is an important characterization method to distinguish D and Q states and reveal the mechanism of REISC.

Corvaja et al. linked C_{60} covalently to a nitroxide radical and constituted a REISC molecule **1**,[73] this is the first example to observe ESP of Q state in solution by TREPR spectra (Fig. 2). The spectra show superposition of three Lorentzian lines centred at

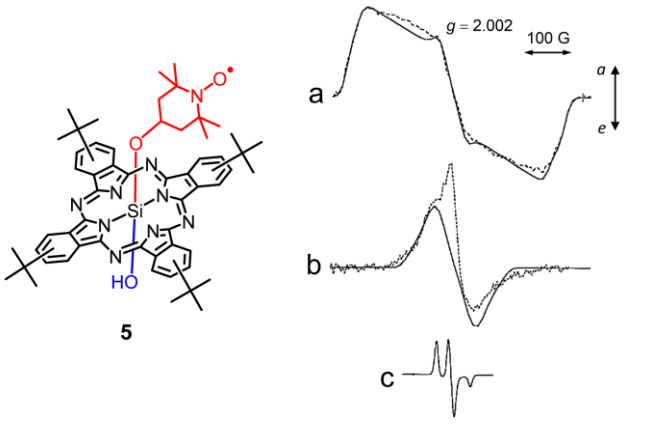

Fig. 4 The molecular structure of porphyrin-TEMPO analogue **5** and TREPR spectra (dotted lines) of (a) reference compound phthalocyaninatosilicon and (b) compound **5** with their simulations (solid lines) and (c) steady-state EPR spectrum of **5**. Reproduced with permission from ref. 79. Copyright 1999 American Chemical Society.

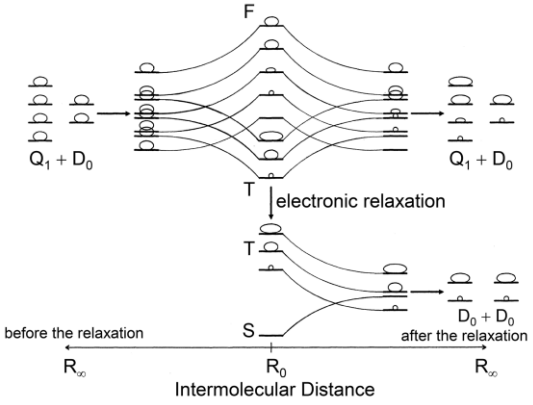

Fig. 5 The radical quartet pair mechanism for rationalization of the ESP of compound **5** upon photoexcitation. Reproduced with permission from ref. 79. Copyright 1999 American Chemical Society.

g = 2.0070 separated by 15.20 G, and other three lines centred at *g* = 2.0043 separated by 5.05 G, the latter can be classified as Q_1 signal (–1/2 ↔ +1/2), other sublevel transition ways are expected to be broadened caused by the rotational diffusion. The time evolution of these two triplet signals at 3346 G and 3366 G are show in inset (a) and (b) of Fig. 2, respectively, although both are fitted by two exponential decay functions (the emission polarized signal at early times represent generation and then change to enhanced absorption), the time constants are different, this supports the conclusion for observation of two different states. The spin polarization of the spectrum can be explained by RTPM mechanism, i.e. the mixing of –1/2 sublevel of D_1 and Q state at the $J > 0$ condition, result in faster inactivation than +1/2 sublevel, therefore, the ISC process produces emission polarization in the beginning, the inactivation of Q_1 is also spin-selective and reverses to –1/2 sublevel, producing enhanced absorption. This is the first example of spin polarization resulting from intramolecular triplet-radical interaction. It should be point out that C_{60} itself has efficient ISC,[46,75] thus from a point of view of designing heavy atom-free triplet PS, it is unnecessary to attach a radical unit to C_{60} to induce the ISC. The major challenge to use C_{60} as heavy atom-free triplet PSs is to enhance its visible light absorption ability.

Yamauchi et al. studied the mechanism of REISC by analyzing the TREPR spectra of several porphyrin and nitroxide radical systems (compound **2** or **3** mixing with TEMPO radical **4**, Fig. 3). The authors proved the co-existence of the ESPT and RTPM mechanisms in the system.[74] The triplet polarizations of porphyrins depend on the central metal atom.[76–78] The peak positions of TREPR spectra of the mixtures are consistent with the steady-state EPR signal of TEMPO (*g* = 2.006, A_N = 15.5) (Fig. 3a), indicating the ESP of porphyrin/TEMPO systems are from TEMPO. The porphyrin/TEMPO mixture exhibits spectra with different polarizations on different delay times (Fig. 3b–e), the polarization in 0.1 – 0.3 μs is consistent with that of the corresponding porphyrin triplet states, the decay time is consistent with the spin-lattice relaxation time of TEMPO radical, which shows the ESP is caused by the ESPT from the triplet state of porphyrin to TEMPO.

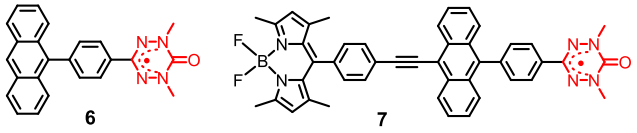

Fig. 6 The molecular structures of Bodipy-phenylanthracene-radical system **7** and phenylanthracene-radical compound **6**.

The polarization of D and Q states at 2.0 – 2.2 μs is caused by the spin-spin exchange interaction of the triplet state and radical, this signal is opposite to that of the porphyrin triplet state, therefore it attributed to the RTPM mechanism of the triplet state precursor ($J < 0$, Q state energy higher than D_1 state). After the addition of ligand pyridine in the porphyrin/TEMPO solution, it has a great influence on the second polarization, the coordination of pyridine disrupts the interaction of TEMPO and porphyrins, indicating the axial coordination on the central metal is important for tuning the RTPM. The TRPER spectra in viscous solvents indicates the polarization is not sensitive to oxygen, but the spin exchange process between the triplet and the doublet states and the rate of ESPT are related to the viscosity of the solvent.

Kobayashi et al. prepared compound **5** by linking TEMPO radicals to phthalocyaninatosilicon framework covalently (Fig. 4).[79] Phthalocyanines are known for their ISC ability.[80,81] The TREPR spectra of **5** in solution observed the opposite polarization of the D (*e* polarization) and Q (*a* polarization) states. The ZFS *D* and *E* parameters of compound **5** triplet state are 2.08×10^{-2} and 5.27×10^{-3} cm^{-1}, which are smaller than that of quartet state of porphyrins without TEMPO (4.3×10^{-3} and 3.3×10^{-4} cm^{-1}) (Fig. 4). The REISC mechanism is shown in Fig. 5, the interaction between the Q and D exciton produces the quintet and triplet states. Due to the electron relaxation, the ZFS effect produces *e* polarization of D state ($J < 0$), which is attributed to radical quartet pair mechanism (RQPM). This spin polarization of D and Q states under the dipole-dipole interaction is intramolecular interaction.

The control of spin alignment of the radicals is very important in the field of organic magnetism. Teki et al. observed the first

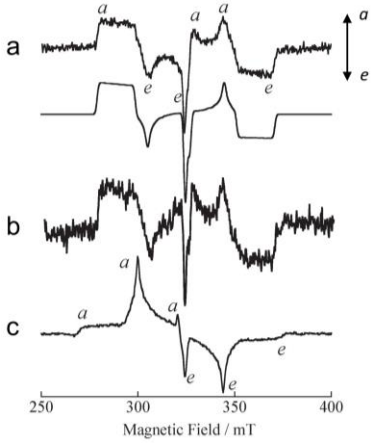

Fig. 7 TREPR spectra of **6** and **7** at 30 K in glass matrix. (a) spectra of **7** with excitation at 505 nm, (b) spectrum of **7** with excitation at 447 nm, (c) spectrum of **6**. Reproduced with permission from ref. 82. Copyright 2008 Royal Society of Chemistry.

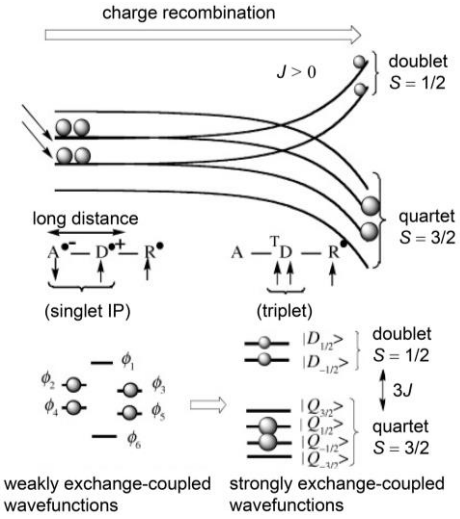

Fig. 8 Mechanism of generation of Q state in **7**. Reproduced with permission from ref. 82. Copyright 2008 Royal Society of Chemistry.

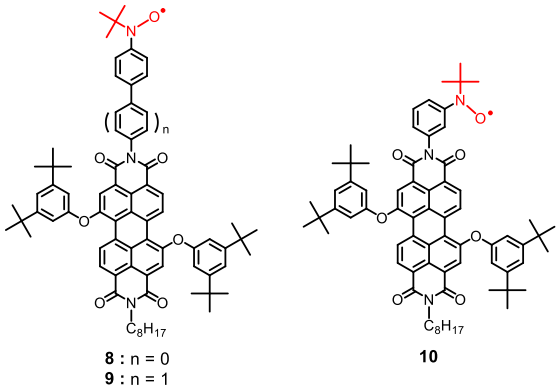

Fig. 9 Molecular structures of PBI–^{2}BPNO$^\bullet$ derivatives.

example of π-conjugated radical spin manipulation via photoexcited ion-pair state (compound **7**, Fig. 6),[82,83] in which phenylanthracene acts as an electron donor and Bodipy acts as an electron acceptor. The polarization and ISC mechanism of the high spin states of **7** were analysed in detail by TREPR spectroscopy. Since the energy transfer from phenylanthracene to Bodipy is efficient, the TREPR spectra of Bodipy and phenylanthracene parts have same ESP pattern (*a, e, e, a, a, e*). The TREPR spectra of reference compound **6** shows the ESP pattern of (*a, a, a, e, e, e*) and its *D* value is 0.0230 cm^{-1}, which is 7% larger than that of compound **7** (Fig. 7). The value of *D* reflects the degree of electron delocalization,[53,76,84] this indicates that the electrons are delocalized to the Bodipy in compound **7**, which further leads to the change of ESP pattern. The spectral pattern of the photoexcited echo-detected EPR spectra of **7** is almost the same as that of TREPR, the spin-echo-detected transient nutation shows the signal is belong to Q state (S = 3/2) with Ms = ±1/2 ↔ ±3/2 transition. The author proposed that the possible photophysical process of **7** is that the singlet excited state populated after photoexcitation, and then a fast photoinduced electron transfer (PET) occurs, resulting in a CS state A$^{\bullet-}$–D$^{\bullet+}$–R. Due to the long distance between donor and acceptor in CS state, the electron exchange

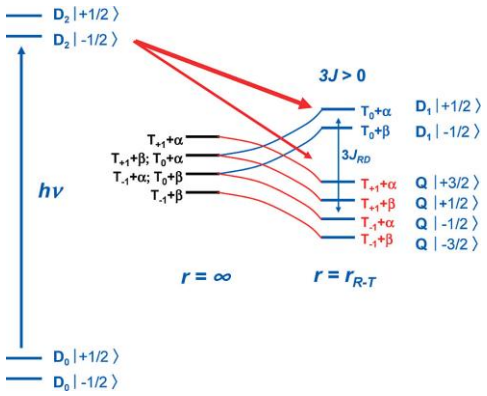

Fig. 10 Simplified energy diagram of PBI–^{2}BPNO$^\bullet$ derivatives **8** and **9**. Thick red arrow represent more rapid ISC than thin red arrow (*J* > 0). Reproduced with permission from ref. 52. Copyright 2009 American Chemical Society.

interaction of A$^{\bullet-}$–D$^{\bullet+}$ is weak, in this case a mixture of D and Q states formed. After the charge recombination, the separation of unpaired electrons decreases and the exchange interaction becomes stronger, REISC effect induce formation of the triplet state in Bodipy part, the whole molecule **7** shows as separated D_1 and Q states. The exchange energy *J* > 0, the D_1 energy is higher than the Q energy, therefore the Q state is selectively populated (Fig. 8). This unique ESP pattern is due to the competition between A$^{\bullet-}$–D$^{\bullet+}$–R and SOC-ISC mechanisms.

The study of a series of PBI–radical derivatives **8–10** by Wasielewski et al. explores the mechanism of REISC. They studied the interactions between PBI and a stable *tert*-butylphenylnitroxide radical (^{2}BPNO$^\bullet$) through ultrafast transient optical absorption and TREPR at high magnetic fields (Fig. 9).[52] Femtosecond transient absorption spectroscopy (fs-TA) indicates the decay of ^{1}PBI in the presence of the radical ^{2}BPNO$^\bullet$ is exceptionally rapid (lifetime of ^{1}PBI state is 4.5 ns). The electronic coupling between these two entities was tuned by varying the distance and orientation of the nitroxide group relative to the attachment position on PBI. As mentioned above, the triplet-spin D_1 and Q states both having two unpaired electrons on PBI, it is difficult to distinguish them by transient absorption spectrum, however, the ISC rate constant can be obtained by monitoring the decay of ^{1}PBI (τ = 2 ps). It is found the electron exchange interaction between ^{1}PBI and ^{2}BPNO$^\bullet$ and the ISC rate depend on the molecular orbital overlap between the orbitals constituting ^{1}PBI and the singly occupied molecular orbital of ^{2}BPNO$^\bullet$. Increasing the distance between ^{2}BPNO$^\bullet$ and ^{1}PBI reduce the overlap, leading to an overall decrease in the yield of ^{3}PBI (for example molecules **8** and **9**), an increase in the distance between the radical and the chromophore by 4.3 Å results in approximately a twofold reduction in the quantum yield of ^{3}PBI, thereby demonstrating that enhancing the electronic coupling drives strong spin-spin interaction will lead to ultrafast ISC. However, in the molecular structure of compound **10**, the π-spin density on the carbon atom connecting ^{2}BPNO$^\bullet$ to PBI is reduced, weakening the overall π-electronic coupling. Yet, the quantum yield of ^{3}PBI of compound **10** is about 25% higher than that of **8**, suggesting that in addition to π-bond interaction, the unpaired electron's

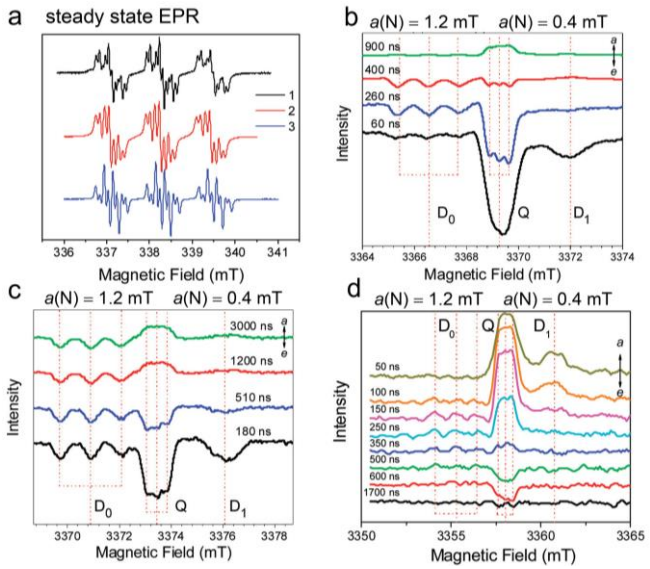

Fig. 11 (a) Steady state EPR and TREPR spectra of PBI–^{2}BPNO$^\bullet$ derivatives (b) **8**, (c) **9** and (d) **10** in toluene at room temperature, measured with W-band spectrometer for (b), (c) and (d). Reproduced with permission from ref. 52. Copyright 2009 American Chemical Society

spin on the nitroxide oxygen can also delocalize through the σ-bond framework via a spin polarization mechanism. These principles maybe used for design of heavy atom-free triplet photosensitizers based on the chromophore-radical molecular structure motif and the REISC mechanism.[85]

The transition of the doublet spin sublevel $D_2 \rightarrow D_1$ (Fig. 10, bold red arrow) is partially allowed since the same multiplicity, the transition of $D_2 \rightarrow Q$ (Fig. 10, thin red arrow) is formally forbidden. Therefore, it is expected a faster $D_2 \rightarrow D_1$ transition than $D_2 \rightarrow Q$ will occur, resulting in a larger initial population of D_1 state as compared to the population of Q state. The TREPR spectra of compounds at the W-band all exhibit spin polarization signals centred at g = 2.0057 (Fig. 11b–d), identical to the ground state signal of ^{2}BPNO$^\bullet$. In toluene at 295 K, the TREPR spectra of these transitions do not exhibit complete anisotropy because the molecular tumbling rate is faster than the timescale corresponding to the energy difference between spin sublevels. Meanwhile, the thermal energy at 295 K is ca. 200 cm^{-1} likely significantly larger than 3J, the RISC from Q to D_1 state (reversed quartet mechanism, RQM) out competes the decay of these states to the D_0 state and the

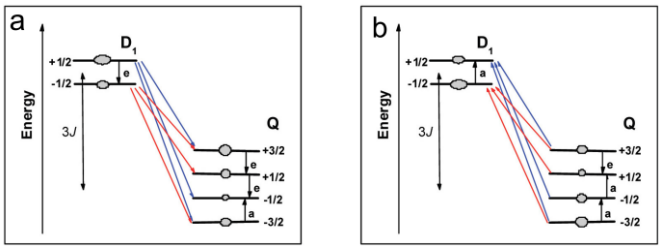

Fig. 12 Mechanism for the electron spin dynamics of **8** and **9** upon photoexcitation. (a) $D_1 \rightarrow Q$ ISC resulting in emissive (*e*) polarization at early time, (b) reversed quartet mechanism $Q \rightarrow D_1$ resulting in enhanced absorption at later time ($J > 0$). Reproduced with permission from ref. 52. Copyright 2009 American Chemical Society.

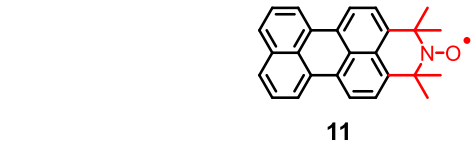

11

Fig. 13 Molecular structure of perylene-radical dyad **11** with short linker between the two units.

relaxation of spin populations back to the Boltzmann distribution.

The TREPR spectra of molecules **8** and **9** indicate the initial polarizations of D_0, D_1, and Q states are emissive. Because these two molecules are ferromagnetic coupling ($3J > 0$), the initial spin energy level populations of D_1 and Q states (Fig. 12a) evolve along with the transition from Q to D_1 state by RQM mechanism (Fig. 12b). Within the 30 ns instrument response functions (IRF), the $D_2 \rightarrow D_1$ transitions is more likely occur than $D_2 \rightarrow Q$ due to the spin-allowed transition, which results in overpopulation of D_1 state. Although D_1 and Q states separated by 3J, the ZFS interaction can mixing these states to some extent, which results in overpopulation of Q state (+3/2 sublevel). That can explain the *e* signals of D_1 and Q states in the initial time. Because the energy gap between Q and D_1 states is much smaller than that of Q and D_0, the $Q \rightarrow D_1$ transition is faster than the $Q \rightarrow D_0$ state. Meanwhile, $D_1 \rightarrow D_0$ transition is spin allowed, these two reasons result in overpopulation of Q state (–3/2). This redistribution of spin populations within D_1 and Q states, along with the relative dissipation rates of D_1 and Q populations to D_0 state, results in the observation of absorptive TREPR transitions at later time, which called ESP revision (Fig. 11). The lifetimes of all subsequent absorptive signals for D_1, Q, and D_0 states in **8** and **9** are longer than those of emission signals, implying their observed lifetimes might actually be limited by spin relaxation. However, the lifetime of ^{3}PBI state measured in toluene using nanosecond transient absorption (ns-TA) spectra (τ_{D2} = 0.54 μs) agree well with the decay constants of absorptive TREPR signals for D_1 (τ_2 = 620 ns) and Q (τ_2 = 410 ns) states. Since the decay of ^{3}PBI state is not affected by spin selectivity and spin relaxation, ns-TA and TREPR spectra show that spin relaxation contributes little to the overall measured TREPR dynamics. A similar situation arises when examining the TREPR spectra dynamics of **10**, except antiferromagnetic coupling, $3J < 0$, inverting the energy ordering of D_1 and Q states, and the temporal order of absorption and emission transitions are also reversed.

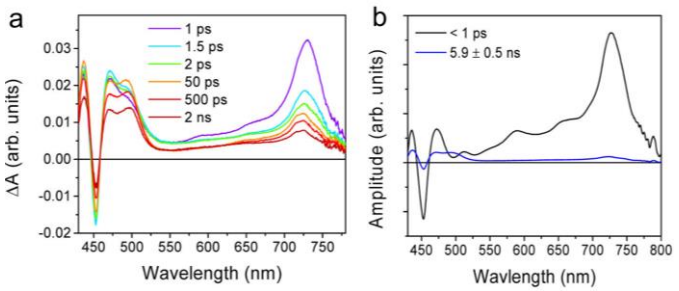

Fig. 14 (a) The fs-TA spectra of compound **11** in toluene. (b) Species associated difference spectra (SADS) obtained through global analysis. Reproduced with permission from ref. 86. Copyright 2015 American Chemical Society.

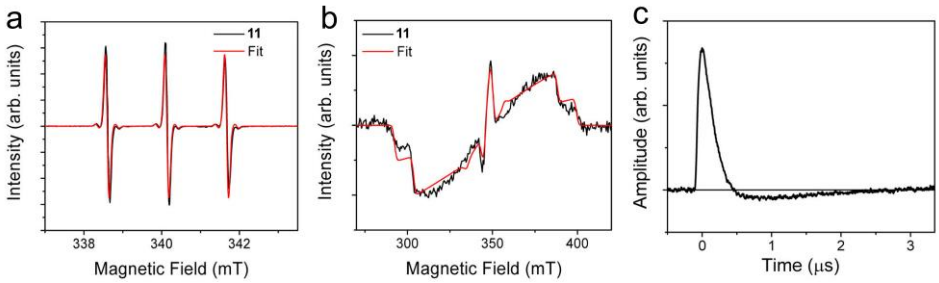

Fig. 15 (a) Steady state EPR spectra, (b) TREPR spectra and (c) decay trace of ESP of compound **11** recorded at 85 K in toluene, (λ_{ex} = 416 nm, 3 mJ/pulse, 9.71 GHz, 6.23 mW). Reproduced with permission from ref. 86. Copyright 2015 American Chemical Society.

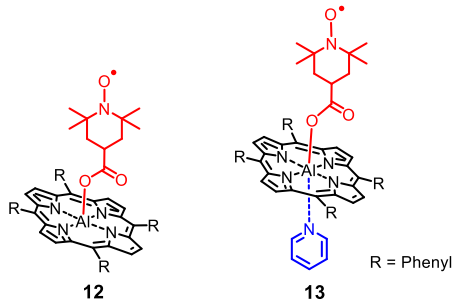

Fig. 16 Molecular structures of aluminum(III) porphyrin–TEMPO complex **12** and ternary structure with coordinated pyridine **13**.

The above example shows that a short linker between the radical and the chromophore is beneficial to improve the REISC efficiency, however, the strong spin interaction may significantly shorten the lifetime. The same research group present a rigid structure **11** of perylene covalently linked to a nitroxide radical (Fig. 13).[86] The S_1 state of perylene is about 3.8 ns, yet the S_1 state lifetime of **11** is less than 1 ps, this is due to the strong spin-spin interaction between the chromophore and the nitroxide radical, the strong coupling also cause the short triplet state lifetime of **11** (7ns, Fig. 14).

The authors studied the steady state EPR spectrum of **11** in toluene at room temperature, which displays a triple lines spectrum with the characteristic isotropic *g* value of 2.00618 and isotropic hyperfine coupling constant of 43.3 MHz (Fig. 15a). The low-temperature TREPR spectrum of **11** exhibits broad and complex features with *e/a* ESP characteristics (Fig. 15b), with the signal undergoing inversion at about 450 ns (as shown in Fig. 15c as negative amplitude), which is fitted to be Q state ($S = 3/2$, $3J >> D$) with $g = 2.0031$, zero-field splitting (ZFS) $D = 750.4$ MHz and $E/D = 0.1942$. Moreover, the TREPR spectrum displays a narrow central peak superimposed on a broad signal. This pattern is characteristic of the Q state in strong coupling regime. The ultrafast REISC under photoexcitation is due to the fast rigid attachment of NO• at a short distance to perylene, resulting in the formation of doublet and quartet states. However, the triplet state lifetime is relatively short, and the molecular structure has not been optimized with the design of triplet state photosensitizers in mind.

Kandrashkin et al. studied the aluminium(III) porphyrin (AlPor) complex covalent with TEMPO axially coordinated on the central metal atom (compound **12** and **13**, Fig. 16).[87] The fluorescence of compounds was quenched by REISC, resulting in D and Q states. At room temperature, the TREPR spectra of **12** show a strong absorption net polarization at 220 ns after photoexcitation, which was assigned as a net polarization of Q state. With elapse of delay time, it evolves into three split narrow signals after 1 μs, by comparing with steady state EPR spectra, the split fine signal is classified as a ground state (D_0) polarization (Fig. 17a). The polarization of the D_0 state is caused by the RQPM mechanism mixing between the Q and D_0 state ($J > 0$). The TREPR spectrum of **12** also show a net polarization at 80 K, and no any multiplet polarization was observed (Fig. 17b). In order to explain this anomalous result, field-swept echo spectrum of the complex was measured without light excitation (Fig. 17c), it is determined that this net polarization comes from the Q state, not the D_0 state, this unusual result suggests that there are other rapid transition processes make the multiple polarization disappear.

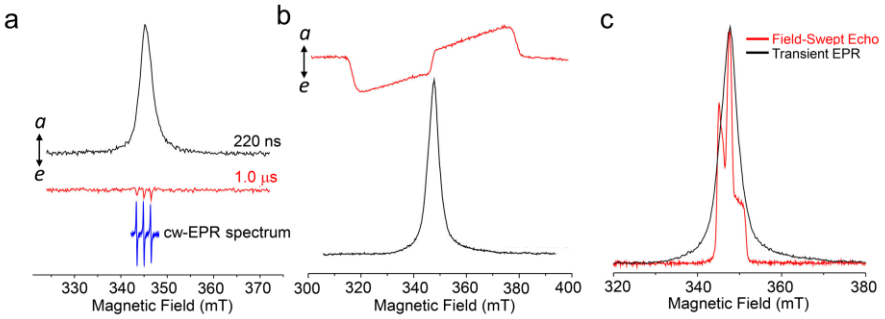

Fig. 17 (a) EPR spectra of complex **12** at 293 K in toluene at different decay time, (b) TREPR of complex **12** (black line) and reference compound without TEMPO (red line), (c) comparison of the TREPR spectra (black line) and the field-swept echo spectrum of the ground state (red) of complex **12** at 80 K in toluene. Reproduced with permission from ref. 87. Copyright 2019 AIP Publishing.

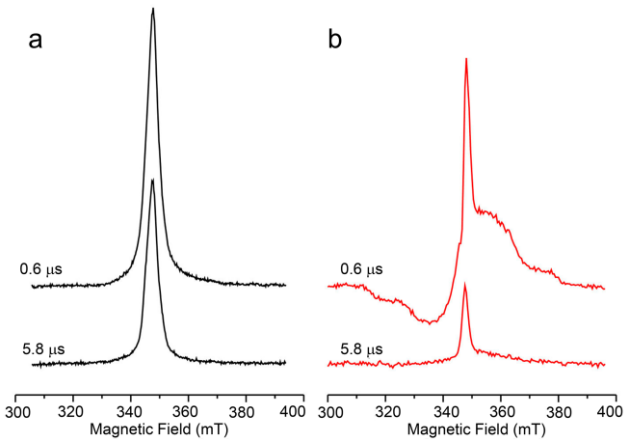

Fig. 18 TREPR spectra of (a) complex **12** and (b) ternary structure **13** coordinate with pyridine at 80 K in toluene. Reproduced with permission from ref. 87. Copyright 2019 AIP Publishing.

It should be noted that the compound can feasibly coordinate with pyridine to form a ternary structure **13** by Lewis acid-base interactions (Fig. 16). It is interesting that the axial coordination of pyridine causes the absorption spectrum redshift and TREPR showing a completely different ESP (Fig. 18). After coordination with pyridine, the polarization signal appeared in the early stage of TREPR spectra at low temperature includes absorptive net polarization and *e/a* multi polarization signal. It is suggested that the polarization mechanism and excited state dynamics of **12** are very sensitive to the changes of π orbital properties of porphyrin molecules. The delocalization of the unpaired electrons of nitrogen oxides and the greater density of π* orbital in the middle of the porphyrin ring indicate that the exchange between the two electrons and the dipole interaction are enhanced by pyridine coordination.

The authors thoroughly analyzed the mechanism of the net polarization. The T_1 and T_2 states of porphyrins are degenerate, so the four-state model (Fig. 19, D_x, D_y, Q_x, Q_y) is considered in this REISC system, the energy gap of Q_x and Q_y (Δ) is somewhat larger than 3*J*. The SOC between D_y and Q_x states and that between D_x and Q_y facilitates the back and forth transitions, the $Q_y \rightarrow Q_x$ transition through internal conversion lead to

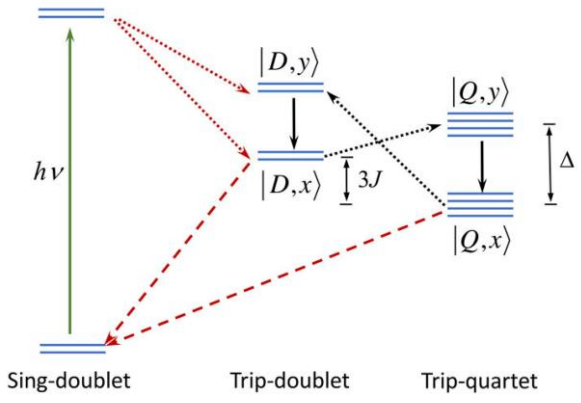

Fig. 19 Simplified energy diagram of aluminium(III) porphyrin–TEMPO system **12** and **13** showing the relaxation pathways. The labels x and y refer to states derived from excitation of an electron from the HOMO into the e_x and e_y orbitals, respectively. Reproduced with permission from ref. 87. Copyright 2019 AIP Publishing.

net polarization and multiple polarization. In compound **12**, the fast balance between D and Q states cause the expected initial multipolarization rapidly decays to strong net polarization within the response time of the spectrometer. When pyridine coordinates, the degeneracy of the two lowest excited states is lifted, resulting in an increase in Δ, this resulted in slower back and forth transitions between D and Q states. This shows that the relative strength of net polarization and multipolarization depends on the rate of equilibrium between D and Q states, and the ESP mode can be tuned by bonding coordination.

The observation and characterization of high-spin states by TREPR spectra provide experimental evidence for the in-depth understanding of the mechanism of REISC, however the design of triplet PSs based on the REISC mechanism should not only consider the generation of high-spin states, but also consider the triplet state lifetime, or the chromophore energy level, even the excited state redox potential, etc.

3. Potential of electron spin polarization in high spin states as qubits or qudits

Advancing molecule-based spintronics focuses on mastering complex multispin system dynamics through photoexcitation, and the molecular systems can be studied with pulsed or time-resolved EPR techniques. Materials with high ESP are gaining interest for applications in quantum information engineering, due to their ability to significantly enhance dynamic nuclear polarization (DNP) efficiency and initialize states for quantum technologies. The unpaired electron spin and nuclear spin in molecules can be used as qubits, which can be regulated by magnetic field effect or microwave pulse to generate ESP and realize quantum information processing.[88,89] The multi-electron high-spin excited states can be used to create entangled spin systems,[26,90–92] this is very important in the field of quantum information science.

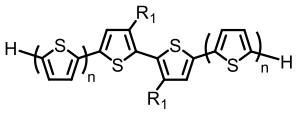

14 : n = 0, R_1 = H
15 : n = 1, R_1 = C_6H_{13}
16 : n = 2, R_1 = C_6H_{13}

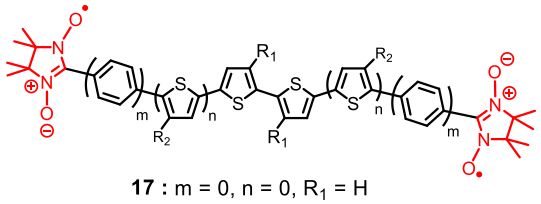

17 : m = 0, n = 0, R_1 = H
18 : m = 0, n = 1, R_1 = C_6H_{13}, R_2 = H
19 : m = 0, n = 2, R_1 = C_6H_{13}, R_2 = H
20 : m = 1, n = 0, R_1 = C_6H_{13}
21 : m = 1, n = 1, R_1 = R_2 = C_6H_{13}
22 : m = 1, n = 2, R_1 = R_2 = C_6H_{13}

Fig. 20 Molecular structures of oligothiophene–diradical and reference compounds.

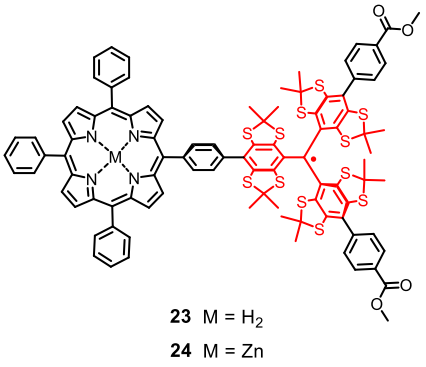

Fig. 21 Molecular structures of the covalently-linked porphyrin-trityl radical compounds.

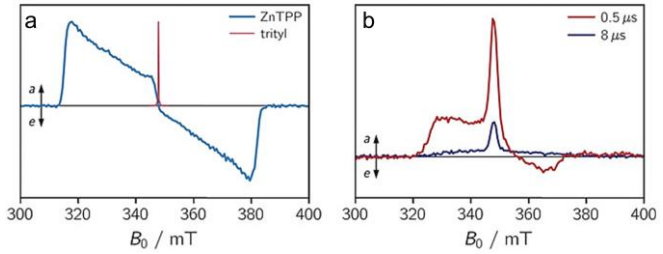

Fig. 22 (a) TREPR spectrum of reference compound ZnTPP and the field-swept FID-detected spectrum of the trityl radical, (b) TREPR spectra of compound **24** at different time delays after photoexcitation, λ_{ex} = 550 nm, X-band (9.75 GHz), 80 K. Reproduced with permission from ref. 94. Copyright 2021 Wiley-VCH.

Controlling the spin dynamics of compounds is important for molecular sensors, spin catalysis, and information technology fields. Wasielewski et al. have reported many studies on photogenerated high spin states as qubits or qudits, which has been summarized in detail in a recent perspective,[26] therefore we will not introduce these work in detail here.

Oligothiophene is a common organic semiconductor material, Lian et al. introduced nitronyl nitroxide (NN) radicals into polymers as a model for probing the dynamics of organic semiconductor excited states, and synthesized a series of oligothiophene-NN compounds **17–22** (Fig. 20).[93] After the introduction of radicals, these molecules have π–π* transition absorption peaks at 365–425 nm, which are consistent with the reference compounds **14–16**, but new n–π* transition absorption peaks appear in the range of 639–707 nm. The fluorescence spectra indicate that the introduction of radicals leads to a complete quenching of the fluorescence. The oligothiophene-NN compounds have strong spin interactions and relatively high antiferromagnetic coupling, and molecule **19** shows smaller antiferromagnetic interactions due to the longer direct distance between the radicals, suggesting that increasing the distance and dihedral angle between the radical and the oligothiophene produces weaker antiferromagnetic interactions. The study shown that enhanced internal conversion (EIC) leads to multiple S, T and Q states of the polymer, the oligothiophenes core can exhibit spin polarization when the radicals and the π–system of the molecule have significant orbital overlap or small distance (<4.3 Å), or intermolecular interactions.

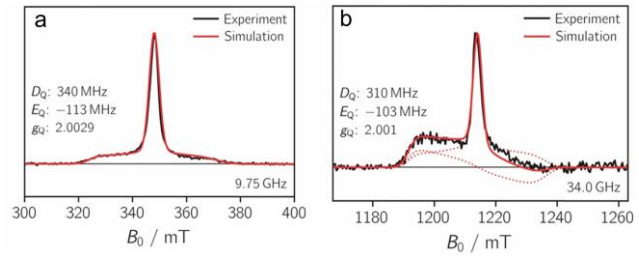

Fig. 23 TREPR spectrum of (a) compound **23** recorded at X-band (9.75 GHz) and (b) **24** at Q-band (34.0 GHz) and simulation line. λ_{ex} = 550 nm, 80 K. Reproduced with permission from ref. 94. Copyright 2021 Wiley-VCH.

Richert et al. reported covalently-linked porphyrin-trityl radical compounds **23** and **24** with a phenyl bridge (Fig. 21).[94] Compound **24** exhibits an efficient energy transfer with the time constant of ~10 ps, as a result, the REISC quantum yield is relatively low, however, TREPR is still able to observe the signal of the spin-polarized state (Fig. 22). The feature and the width of TRPER spectral signal for **24** at X-band (9.75 GHz) is different with the spectra of the two building blocks, the wider *a/e* spin polarization in short time scale can be assigned to the multiplet polarization of Q state (caused by the transition of $|\pm 1/2\rangle \leftrightarrow |\pm 3/2\rangle$), the residual central enhanced absorption peak in 8 μs can be assigned to transitions between the +1/2 and −1/2 sublevels of the Q state, called net polarization for the Q state in thermal equilibrium, the positive net polarization implying positive J_{TR} value in **24**, the Q state is lower in energy than the D_1 state. It should be pointed out that no any D_1 state signal can be recorded, it is probably due to the fast relaxation between D_1 and Q states and the efficient inactivate for D_1 state to D_0 state.

The TREPR spectra of **24** were also record at Q-band (34.0 GHz), the qualitative similarity of the signal at different frequency indicated the electron spin-spin exchange interaction

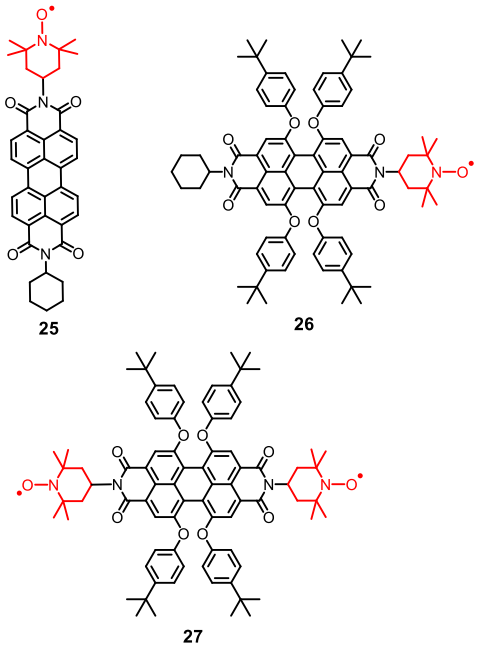

Fig. 24 Molecular structures of the PBI-TEMPO derivatives **25**, **26** and **27**.

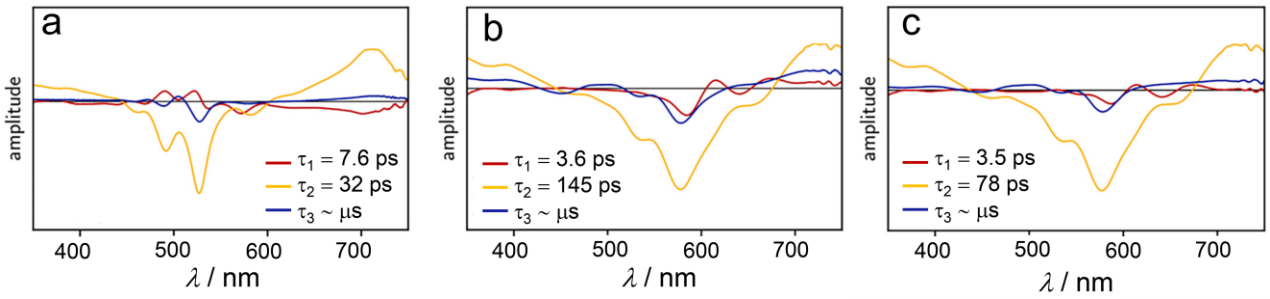

Fig. 25 Decay associated difference spectra and time constants obtained from a global kinetic analysis of the fs-TA spectral data of compounds (a) **25**, (b) **26** and (c) **27**. Reproduced with permission from ref. 55. Copyright 2022 Royal Society of Chemistry.

between ZnTPP and trityl radical is strong, despite of the presence of the phenyl spacer between the two units (Fig. 23). When the metal atoms in the porphyrin centre are removed, the free base porphyrins show non-symmetric and non-planar structure, different conformation or symmetry will lead to different TREPR spectra. There is only net polarization observed for **23**, indicated the symmetry breaking leads to a much larger splitting between Q sublevel, cause faster equilibration kinetics between D_1 and Q states (Fig. 23).

PBI chromophores **25** – **27** covalent attached with either one or two TEMPO to the imide position(s) can form high spin states effectively (Fig. 24).[55] The fs-TA spectra of the chromophores elucidated that, the radical can shorten the lifetime of S_1 state significantly and transform the radiative transition pathway of the S_1 state into nonradiative transition, for instance, ISC process, electron transfer or energy transfer, etc (the lifetime of S_1 state is beyond the time window of fs-TA spectrometer for the parent PBI chromophore, Fig. 25). Therefore, the derivatives containing the free radicals may show formation of triplet state in the fs-TA spectrum (the formation of triplet state was not observed for the unsubstituted PBI). The global analysis of the fs-TA spectra gives the time constants of the excited state deactivation of the compounds, fast ISC rate k_{ISC} (the time constant of ISC is τ_2 in Fig. 25) of PBI derivatives indicate the ISC dominate the deactivation of the S_1 state, the quantum yield of the triplet state is increased from almost zero to over 50% in toluene. Compound **26** has four times slower formation of triplet state as compared with **25** (τ_{ISC} of **26** is 110 ps, τ_{ISC} of **25** is 27 ps, Fig. 25). The evaluate about the possibility of the electron transfer and energy transfer indicated that, electron transfer in these systems is possible although no signals of anions and cations were observed in the transient absorption spectrum, it is due to the rapid charge recombination to the chromophore triplet state. For compound **25** competing Förster-type energy transfer and ISC co-exist. After connecting the second TEMPO (compound **27**), the k_{ISC} can be further accelerated (1.2×10^{10} s^{-1}).

The charge recombination facilitates triplet state generation can also be demonstrated by TREPR spectral experiments, PBI-TEMPO systems show anomalous ESP pattern (*a, e, e, a, a, e*), indicating that it is not caused by normal SOC effect (Fig. 26). Compounds **25** and **26** belong to strong coupling systems, TREPE spectra demonstrate the pure Q state multiplet polarization at outer wings corresponding to the transition $|\pm 1/2\rangle \leftrightarrow |\pm 3/2\rangle$, with an overpopulation of $m_s = |\pm 1/2\rangle$ (Fig. 26). The TREPR spectra of **27** shows small difference with **26** on the relative intensity of the signal, that maybe caused by a small number of quintet formation with the spin exchange interaction of PBI and two radicals. In addition, the transient nutation frequency experiment also confirm the quintet state formation.

In the REISC system, the S_1 state is usually deactivated by competitive electron transfer or energy transfer processes. In order to enhance the efficiency of REISC, reducing the relaxation of the S_1 state by other pathways should be considered. Adjust redox potential will affect the Gibbs free energy of electron transfer, appropriate modifications can affect the absorption wavelength to weaken the overlap between the luminescence spectrum of energy donor and the absorption spectrum of energy acceptor, thereby weakening energy transfer. For the modification of PBI, attachment of the free radicals at the core position rather than the imide position can make the transition dipole moment of free radicals perpendicular to the chromophore, which is benefits to limit the energy transfer process.

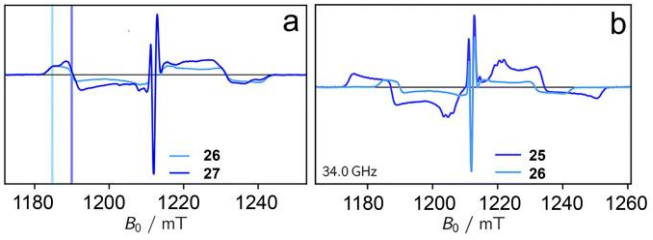

Fig. 26 Comparation of the TREPR spectra of compounds (a) **26** and **27**, (b) **25** and **26** in frozen toluene solution at 80 K. Reproduced with permission from ref. 55. Copyright 2022 Royal Society of Chemistry.

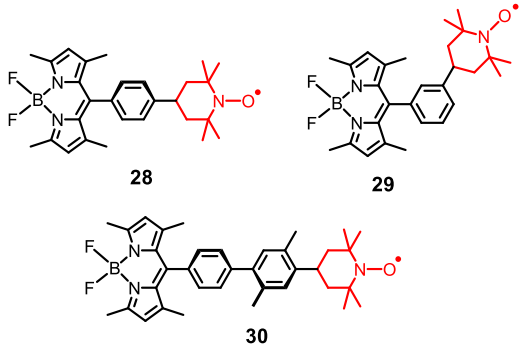

Fig. 27 Molecular structures of the Bodipy-TEMPO derivatives **28**, **29** and **30**.

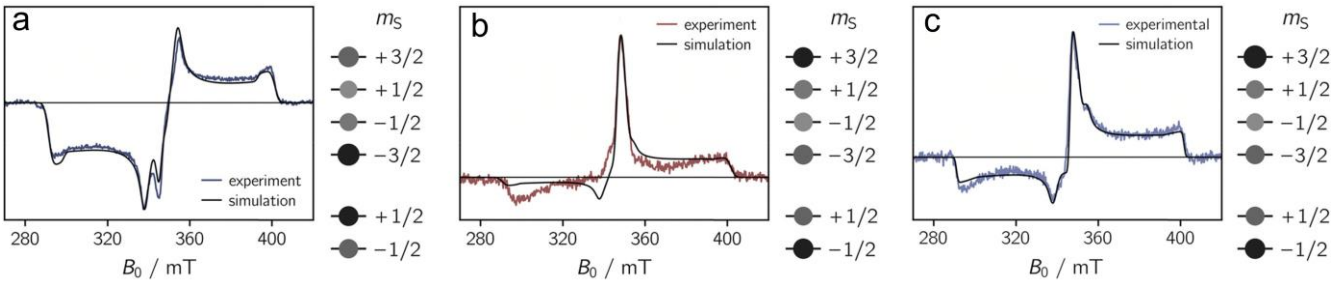

Fig. 28 TREPR spectra of the Bodipy-TEMPO derivatives (a) **28**, (b) **29** and (c) **30** together with numerical simulations of the data. The relative populations of the D_1 and Q sublevels are indicated by the shade of color. Reproduced with permission from ref. 56. Copyright 2023 Royal Society of Chemistry.

Along this line, a series of Bodipy–nitroxide dyads **28–30** were synthesized by attaching TEMPO radical to *meso* position of Bodipy (Fig. 27),[56] TD-DFT calculations demonstrate that the transition dipole moments of **28**, **29** and **30** are oriented along the *N*–*N* direction of Bodipy, which is perpendicular to the chromophore–radical bonding axis, such molecular design idea can block energy transfer effectively. Studies of these compounds have shown that different separation distances and relative orientations of radical and chromophore represent different REISC performance. The singlet oxygen quantum yield of **29** is the highest in these three compounds (Φ_Δ = 23%), because the REISC is mediated by dipolar interaction between chromophore and radical, which is dependent on the distance between the two units. The longest distance of separation is achieved by using two phenyl rings in **30**, which shows negligible REISC (Φ_Δ = 2%). Compound **28** have moderate REISC quantum yield (Φ_Δ = 12%). The TREPR spectra of these three compounds all show the mixture of multiplet polarization and net polarization of Q state (Fig. 28), the difference is the net polarization of $|+1/2\rangle \leftrightarrow |-1/2\rangle$ for **28** is opposite with the other two compound. There is no simple correlation between the polarization intensity of the Q state and the REISC efficiency (**29** show the most efficient REISC, but the TREPR signal is the weakest), means a higher REISC efficiency cannot guarantee the generation of more polarized Q states. The magnitude of the exchange coupling interaction (J_{TR}) will affect doublet–quartet mixing mechanisms, this makes the mechanism of high spin states obtained by REISC system complex.

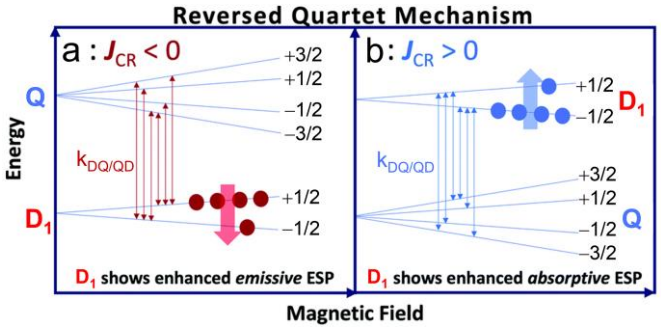

Fig. 29 The RQM mechanism with (a) antiferromagnetic coupling $J_{CR} < 0$ and (b) ferromagnetic coupling $J_{CR} > 0$. Spin-selective transitions between D_1 and Q states result in non-Boltzmann population, leading to emissive or enhanced absorptive ESP. Reproduced with permission from ref. 67. Copyright 2021 Royal Society of Chemistry.

It is generally believed that in the RQM mechanism, the sign of ESP of the ground state can be regulated by changing the sign of spin exchange interaction between chromophore and free radical, J_{CR} (that is, variation between ferromagnetism and antiferromagnetism character). If the decay rate of the D_1 state to D_0 state is faster than that of T_1 spin relaxation of the appended radical in the D_0 state, the ESP will transfer from the excited state to the D_0 state of radical. In the antiferromagnetic system ($J_{CR} < 0$), the Q state is higher in energy than D_1 state, the ZFS mixing of Q and D_1 state will result the overpopulated of Ms = +1/2 sublevel, and emissive ESP will be observed. On the contrary, in the ferromagnetic coupling system ($J_{CR} > 0$), the overpopulated of Ms = −1/2 sublevel will cause an enhanced absorptive ESP (Fig. 29).[67] However, a series of studies have shown that the ESP is affected not only by changing the sign of J_{CR}, but also by structure−property relationships.

REISC system utilize the ligand to ligand electron transfer (LL'CT) state as a precursor is easier to regulate because this state is more sensitive to the environment (e.g., solvent media) and it is easy to control spin polarization. Est et al. reported a series of nitronyl nitroxide (NN) radical-elaborated donor (catecholate, CAT)-acceptor (4,4′-di-tert-butyl-2,2′-bipyridine, bpy) complexes **31** and **32** with different metal center, ligand (CAT)-to-ligand (bpy) charge transfer (LL'CT) upon photoexcitation will occur in these molecules (Fig. 30).[65,67] The control molecule lacks the electron acceptor ligand NN, there is no LL'CT property and no ESP signal is observed, indicating that LL'CT is indispensable in this ESP mechanism. **31** and **32** have the same molecular framework, except for metal atoms, but lead to completely different ESP behaviors. An enhanced absorption ESP is observed in the D_0 state of **32**, while a very weak emission ESP is observed for **31** (Fig. 31). This phenomenon can be explained by different mixing mechanisms in **31** and **32**, the chromophore−radical exchange ($J_{SQ\text{-}NN}$) is antiferromagnetic,

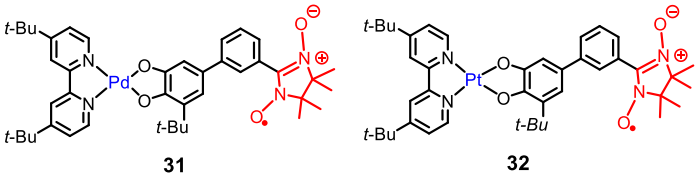

Fig. 30 Molecular structures of the NN radical-CAT-bpy complexes **31** and **32**.

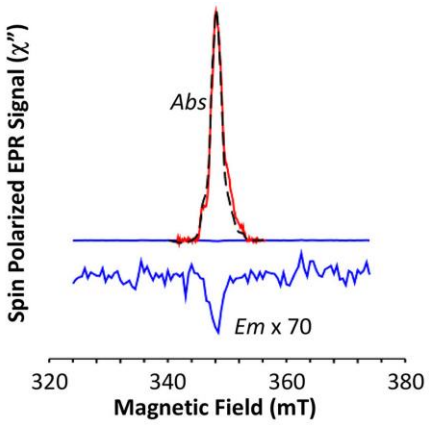

Fig. 31 TREPR spectra of complexes **31** (blue lines) and **32** (red lines) at 20K, $\lambda_{ex} = 532$ nm. The dashed black line is the integrated and normalized steady state EPR spectrum of **32** for comparison. Reproduced with permission from ref. 65. Copyright 2021 American Chemical Society.

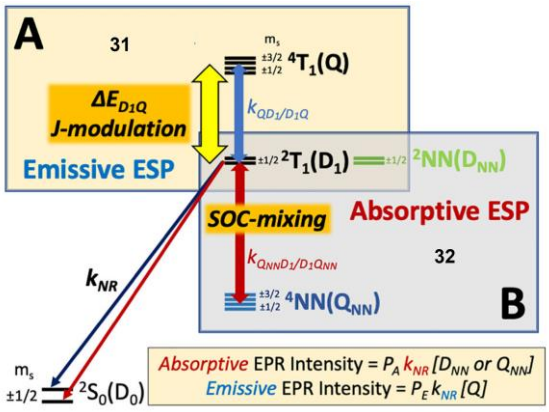

Fig. 32 The RQM mechanism of complexes **31** (A mechanism: D_1 and Q states mixed by $J_{SQ\text{-}NN}$ modulation gives the emissive ESP of D_0 state) and **32** (B mechanism : spin–orbit-coupling mix the D_1 and the NN-based quartet state, ^{4}NN, gives the absorptive ESP of D_0 state. Reproduced with permission from ref. 65. Copyright 2021 American Chemical Society.

that means the energy level of D_1 state being lower than the Q state (Fig. 32), the RQM mechanism caused the thermal population of the Q state and ZFS-induced mixing of the D_1 and Q states, the Ms =+1/2 sublevel will be overpopulated, this produces an emissive ESP in the excited states. Since D_1 to the ground state is spin allowed, a fast decay of $D_1 \rightarrow D_0$ will retain the ESP to ground state (mechanism A). The mechanism A can explain the TREPR spectral result of **31**. The differences between **31** and **32** lie in the magnitude of their metal ion SOC constant ($\delta_{Pt} \approx 4508$ cm^{-1} for Pt, $\delta_{Pd} \approx 1504$ cm^{-1} for Pd), the stronger SOC effect in **32** leads to the strong mixing of D_1 and ^{4}NN/^{2}NN states (theoretical calculation indicated that the D_1

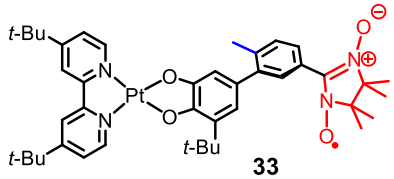

Fig. 33 Molecular structure of the Pt(II) complexes **33**.

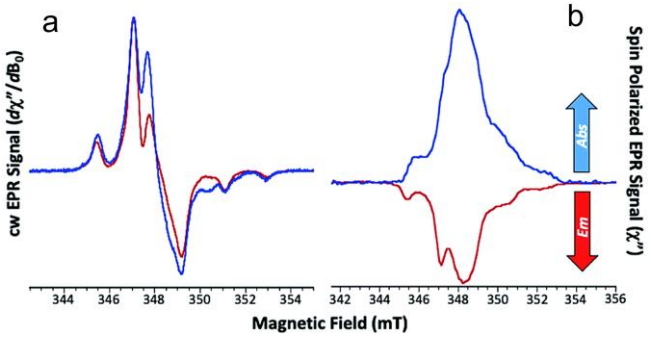

Fig. 34 (a) Steady state EPR spectra of the ground states and (b) TREPR spectra of **32** (blue lines) and **33** (red lines), $\lambda_{ex} = 532$ nm at X-band. Reproduced with permission from ref. 67. Copyright 2021 Royal Society of Chemistry.

and ^{4}NN/^{2}NN states are close to each other, Fig. 32), these conditions allow the appearance of strong absorptive ESP in the D_0 ground state (mechanism B). This example confirms that different metal with different SOC effect, leading to different ESP on both the sign and amplitude in the D_0 states following photoexcitation.

In addition to the influence of the central metal, the conformation between the radical and the chromophore also affects ESP. A single methyl substituent on the *meta*-phenylene bridge results in increased bridge bond torsion in the molecular structure of compound **33** (Fig. 33), the torsion result in twisted conjugated structures which will reduce the $J_{SQ\text{-}NN}$ ($J_{SQ\text{-}NN} = 2J_{CR}$), further results in $\Delta E_{D1/Q}$(**33**) < $\Delta E_{D1/Q}$(**32**).[66,67] In the TREPR spectra, the ground state ESP signals of the **32** and **33** were observed (Fig. 34), different from the traditional results of predicting ESP symbols based on the sign of J_{CR} value, different ESP signals are observed, although both compounds are antiferromagnetic coupling systems. TREPR spectra indicate the emissive ESP in the **33** and enhanced absorptive ESP in the recovered ground state of **32** (Fig. 34). The author estimated the $\Delta E_{D1/Q}$ (**32**) is 48 cm^{-1} and that for **33** is 6 cm^{-1}, respectively. Although Pt atom has a larger SOC constant, the smaller $\Delta E_{D1/Q}$ in **33** translates the mechanism into mechanism A (Fig. 35), that is, ZFS promotes the generation of emissive ESP under the conformation limitation of methyl groups.

The methyl group on the bridge can regulate the torsion angle between chromophores and radical, thus affect the strength of electron coupling interaction (compounds **34** –**38**, Fig. 36).[92] Compound **34** has tetramethylphenyl as bridge between Pt centre and NN radical , the large torsion angle dramatically reduce $J_{SQ\text{-}NN}$ in the excited LL'CT state, resulted in a small $\Delta E_{D1/Q}$ that benefit for greater mixing of the D_1 and Q states (Fig. 37). Unlike the control molecule **38** shows ferromagnetic exchange between the NN and SQ radicals. Under the RQM mechanism, the Q-state energy of these two compounds is slightly lower than that of D_1 state, the ZFS mixing effect will generate the absorptive ESP signal of the excited state, the strong mixing of D_1 and Q states promotes the non-radiative relaxation of D_1 state to the ground state, and the spin polarization generated in the excited state is more effectively transferred to the ground state of **34** (D_0 state). Therefore, the TREPR spectrum of **34** show a stronger absorption signal as

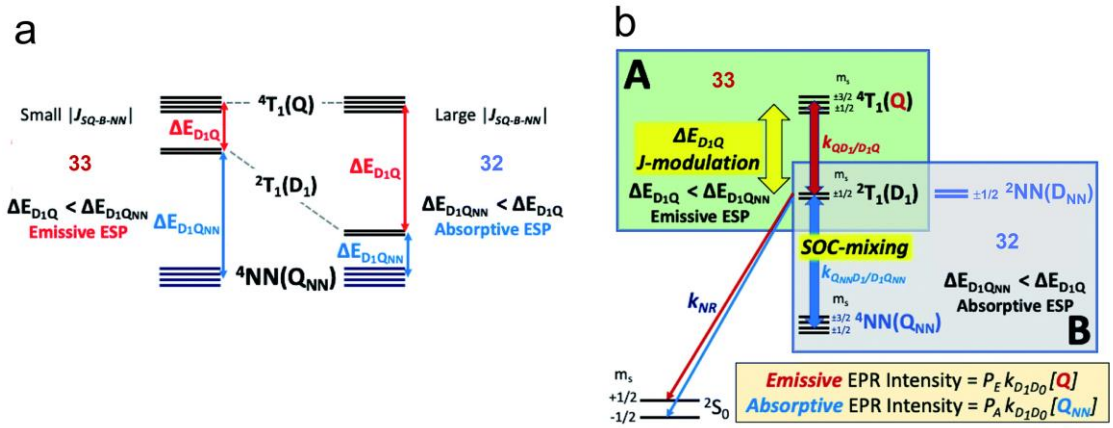

Fig. 35 (a) Origins of ESP and (b) the RQM mechanism of complexes **33** (A mechanism : D_1 and Q states mixed by $J_{SQ\text{-}NN}$ modulation gives the emissive ESP of D_0 state) and **32** (B mechanism : spin–orbit-coupling mix the D_1 and the NN-based quartet state, ^{4}NN, gives the absorptive ESP of D_0 state. Reproduced with permission from ref. 67. Copyright 2021 Royal Society of Chemistry.

compared with **38** (Fig. 38). This is an example of regulating ESP by limiting the torsion angle between radical and chromophore through the steric hindrance effect of methyl groups on the linker, further demonstrating the importance of molecular structure to construct the ground state qubits.

It should be pointed out that molecules with Pt(II) coordinate framework usually show efficient ISC and the compounds have been used as triplet PSs.[95,96] Attaching of radical unit to the transition metal complex molecular structure may shorten the triplet state lifetime.[97,98] The ESP of chromophore-radical dyads containing flexible linker has been studied for a long time.[100,101] Yanai et al. introduced a flexible linker in the hybrid systems **39–42** of porphyrin and TEMPO to achieve efficient and persistent ESP.[99] The structural flexibility of the linker altered the interaction between the radical and triplet states, promoting the ESP by bringing the free radical and the triplet state closer while avoiding rapid relaxation due to strong interaction (Fig. 39). The results showed that the ESP of the triplet state of this hybrid system exceed that of the unlinked system, with ESP duration exceeding 10 μs.

To compare the impact of free radicals on singlet state quenching, the authors investigated the non-radiative transition rate k_{nr}, the k_{nr} values of the hybrid system were significantly larger than those of the unlinked system. Interestingly, the k_{nr} values for the dyads (**41** and **42**) containing longer linkers were slightly larger compared to those with shorter linkers (**39** and **40**).

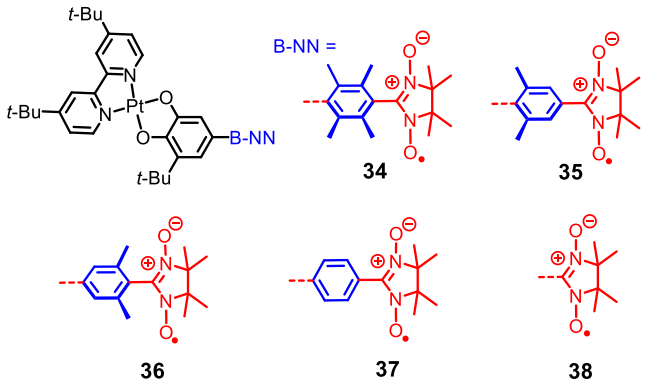

Fig. 36 Molecular structures of NN radical-CAT-bpy complexes with different torsion angle.

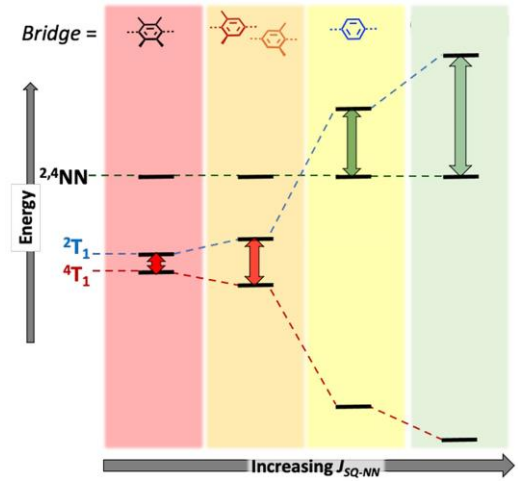

Fig. 37 RQM and modified RQM mechanisms and energy level of compounds **34 –38**. Red and orange panels: weak $J_{SQ\text{-}NN}$ modulation gives the ESP derived from the equilibrium of D_1 and Q states. Yellow and green panels: strong $J_{SQ\text{-}NN}$ derived from equilibrium with the localized radical excited states, ^{4}NN and/or ^{2}NN. Reproduced with permission from ref. 92. Copyright 2022 American Chemical Society.

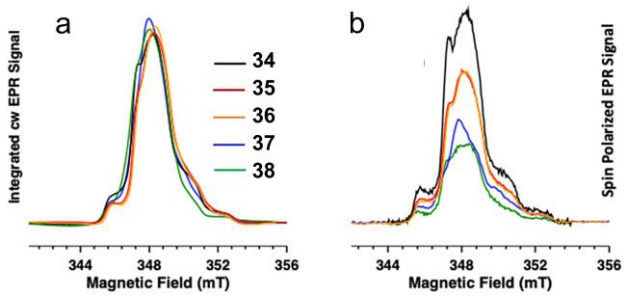

Fig. 38 (a) Steady state EPR spectra of the ground states and (b) TREPR spectra of **34** (black lines), **35** (red lines), **36** (orange lines), **37** (blue lines) and **38** (green lines), λ_{ex} = 532 nm at X-band. Reproduced with permission from ref. 92. Copyright 2022 American Chemical Society.

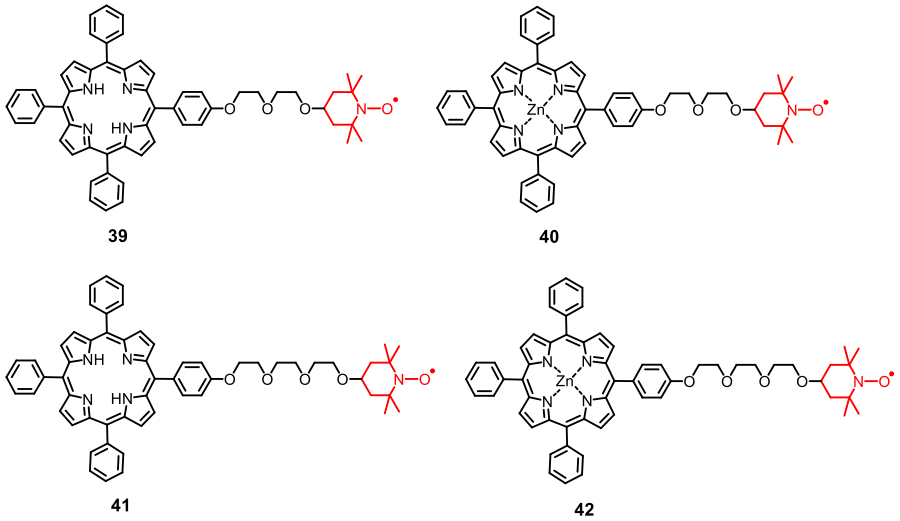

Fig. 39 Molecular structures of hybrid porphyrin-TEMPO systems **39–42** with flexible linker.

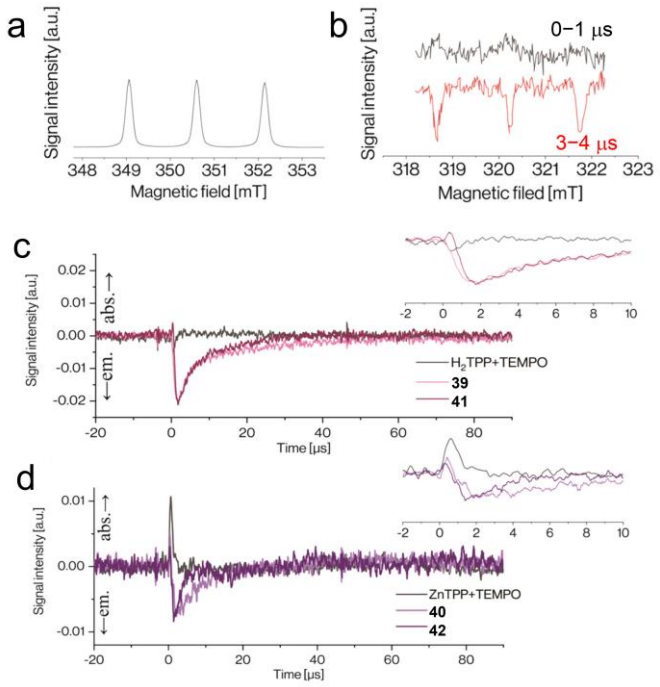

Fig. 40 (a) Steady state EPR spectrum and (b) TREPR spectra of **41** (black line: 0–1 μs, red line: 3–4 μs), (c) time-evolution of the EPR signal at 321.8 mT of **41** (red line) and **39** (pink line), and unlinked mixture of H_2TPP and TEMPO (black line) in toluene, (d) time-evolution of the EPR signal at 321.8 mT of **42** (dark purple line) and **40** (light purple line), and unlinked mixture of ZnTPP and TEMPO (black line) in toluene. Reproduced with permission from ref. 99. Copyright 2023 American Chemical Society.

The authors investigated the polarization mechanism of the system through TREPR spectral studies (Fig. 40). Emission signals were observed for unlinked mixture of H_2TPP and TEMPO, while absorption signals were observed for the mixture of ZnTPP and TEMPO, reflecting different possible ESP mechanisms. For the emission ESP signal, the authors proposed a mechanism of RTPM or related RQPM, as the free radical decay in the system reached several tens of microseconds (Fig. 40). The emissive TREPR signal could be attributed to the hyperpolarized nitroxide free radical, with the duration of the emission signal exceeding the spin-lattice relaxation time (<1 μs).[102] Due to the chromophore and free radical being connected by a relatively long, flexible linker, this flexibility would allow diffusion, leading to intramolecular RTPM. In the hybrid system, the distance between porphyrin and TEMPO is minimized in the folded form. As a result, quartet and doublet states are formed due to the strong exchange interaction, as opposed to the Zeeman effect observed in the folded form. On the other hand, in the extended form, the distances between **39**/**40** and **41**/**42** are respectively 12 and 14 Å, which weakens the interaction and leads to the formation of triplet and doublet states.

The absorptive signal decayed within 1 μs, close to the spin-lattice relaxation time of the D_0 state of the nitroxide free radical, indicating the occurrence of ESPT. It was found that the excited triplet state of ZnTPP has positive polarization. The absorption signals in the ZnTPP hybrid systems (**40** and **42**) may be attributed to ESPT. However, since the triplet state of H_2TPP is known to have negative polarization, another possible reason for the absorption signal generation is the RTPM from the singlet excited state S_1 of the porphyrin to the radical unit. The excited state then rapidly relaxes to the D_1 state due to enhanced ISC. ESP arises from the mixing of the doublet state D_1 and quartet state Q_1 during the separation process.

In this hybrid system, linking of a radical unit to a chromophore shortens the fluorescence lifetime, suggesting that the singlet state might be quenched by the radical, leading to absorptive ESP signals based on the RTPM with singlet excited state. They discovered that longer linkers can quench the dye's excited state with radicals more effectively while still maintaining a longer triplet state lifetime. Therefore, by introducing a flexible linker, both efficient and persistent ESP maybe achieved simultaneously.

4. Molecular design strategy of REISC systems as triplet photosensitizers

In REISC systems, the relaxation of D_1 state to the ground state ($D_1 \rightarrow D_0$) is spin-allowed transition, thereby shortening the lifetime of the excited states of the chromophore (triplet spin multiplicity). The radicals can promote the generation of triple states based on REISC, but they also shorten the lifetime of triplet excited states of the chromophore. The stronger the interaction between radical and chromophore, the higher the ISC efficiency, but the triplet state lifetime of the chromophore will be shortened. Increasing the distance between radical and chromophore can prolong the triplet state lifetime, but the ISC efficiency will be sacrificed. Thus, long triplet state lifetime and high ISC efficiency of the REISC system cannot be achieved simultaneously. There is still much room for the molecular design of triplet state photosensitizers based on REISC, it is important to tune the electron exchange interaction magnitude to realize long triplet state lifetimes and high triplet state quantum yields at same time. A possible answer for this problem is to use flexible chains to connect the radical and the chromophore to have multiple conformations and makes the intermolecular contact of the radical and chromophore to be in transient character, thus making it possible to achieve.

In view of this rationale, we used flexible chains to connect TEMPO radicals with Bodipy chromophore and investigated the effect of this flexible linkage on the triplet state properties in detail (**43** and **44**, Fig. 41).[70] Bodipy is one of the mostly studied chromophores, due to the desired photophysical property, such as significant visible light absorption and high fluorescence yield, as well as the feasible derivatization. Its potential application in design of triplet PSs has not been fully explored. The photophysical properties of **43** and **44** were investigated using steady-state and time-resolved transient optical spectroscopy. Spin interactions between the chromophore and radicals resulted in significant quenching of the fluorescence of Bodipy, this interaction also produced D and Q states. Spin-polarized TEMPO signals generated by the RTPM mechanism were observed in the TREPR spectra of **43** and **44** (Fig. 42). The enhanced absorption spin polarization caused by the free radical-induced $S_1 \rightarrow T_1$ process was observed at delay time of 0.3 μs, the Bodipy moiety reaches a singlet excited state upon photoexcitation and forms a doublet state by interacting with free radicals. Due to the electron spin exchange, the free radical induces the intersystem crossing to form a triplet state, and the whole spin states of the molecule are D_1 state and Q state (Fig. 42). When the electron exchange energy (*J* value) of this system is negative, the quartet energy level of the whole system is higher than the doublet energy level, and the $D_2 \rightarrow D_1$ process will lead to the excess distribution of D_1 state. After the

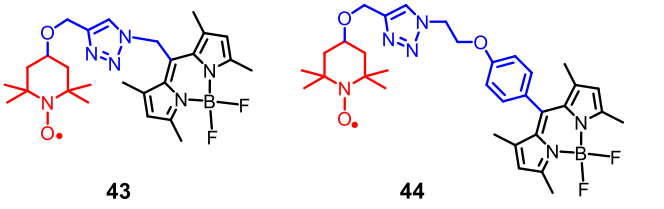

Fig. 41 Molecular structures of Bodipy-TEMPO dyads **43** and **44** containing flexible linkers.

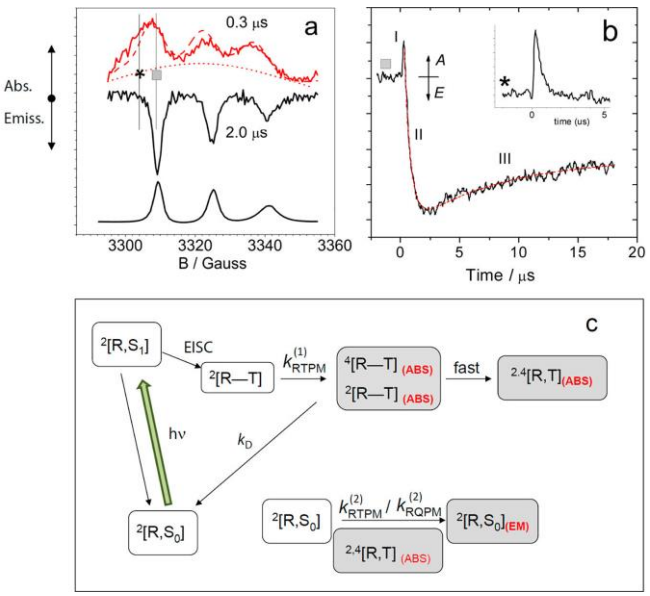

Fig. 42 (a) TREPR spectra of **43** in toluene at different delay times of 0.3 μs (red, top) and 2 μs (black, medium) at 185 K. The bottom spectrum in (a) is the steady state EPR spectrum (g = 2.0063). (b) Decay curve taken at 3309 G (■ in graph (a)) and fit by using biexponential functions based on the RTPM mechanism (red dashed line). (c) Simplified mechanism of REISC generate D_1 and Q states of **43**. Reproduced with permission from ref. 70. Copyright 2017 American Chemical Society.

mixing of D_1 and Q states, it will lead to *a* spin polarization of these two states. That is, the RTPM mechanism with the doublet D_1 as the precursor. At delay time of 2.0 μs, the emissive spin polarization was observed, which is caused by $D_1 \rightarrow D_0$ process (g = 2.0064, a_N = 15.8 ± 0.1 G), the splitting character is consistent with the steady state EPR spectrum of **43** (g = 2.0063, a_N = 15.75±0.05 G). This *e* spin polarization is caused by the radical-induced $D_1 \rightarrow D_0$ process, as shown in Fig.42. Due to the negative electron exchange energy of the system, the rapid deactivation of $Q \rightarrow D_0$ makes the quartet state get more population. After the mixing of D_1 and Q states, it will lead to the *e* spin polarization of these two states. The *e* spin polarization of the ground state TEMPO radical is produced by the intermolecular RTPM mechanism or the radical quartet state pair mechanism (RQPM).

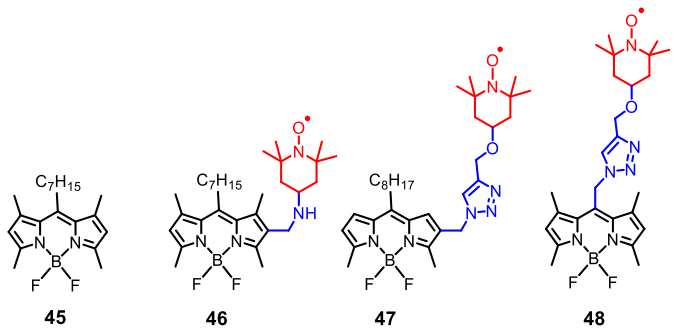

Fig. 43 Molecular structures of Bodipy-TEMPO dyads **46**–**48** containing flexible linker and reference compound **45**.

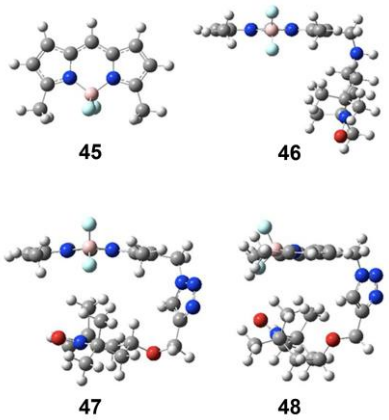

Fig. 44 Ground state geometries of chromophores **46**–**48** obtained by DFT calculation. Reproduced with permission from ref. 103. Copyright 2020 AIP Publishing.

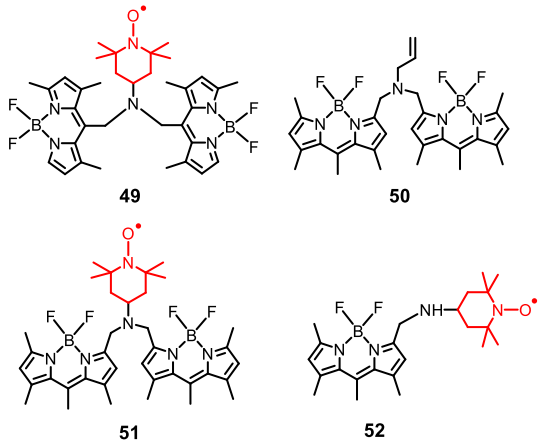

Fig. 45 Molecular structures of Bodipy dimer-TEMPO compounds **49** (the expected molecular structure), **51** (experimentally isolated major product) and **52** and reference compound **50**.

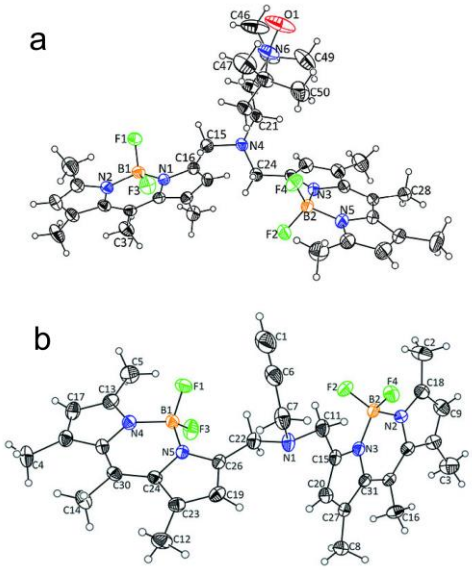

Fig. 46 ORTEP views of the molecular structures determined by single-crystal X-ray diffraction of (a) **51** and (b) **50** (thermal ellipsoids drawn at the 30 % probability level). Reproduced with permission from ref. 104. Copyright 2018 Wiley-VCH.

The results of ns-TA spectra indicate that a high triplet state quantum yield of Φ_T = 80% and an exceptionally long τ_T = 62 μs were achieved for **43** with the shorter flexible linker, due to a suitable spin-spin interaction magnitude between the chromophore and the radical. **44** containing a longer linker chain gives a lower ISC efficiency (Φ_T = 14%), but a longer triplet state lifetime (190 μs). Therefore, it is critical to tune the molecular structure to attain decant triplet-state quantum yield and the triplet state lifetime simultaneously. Our group first proposed the concept of using a flexible linker with appropriate length may become one method to design the molecular structure of triplet PSs based on REISC mechanism, which is important for the design of novel triplet PSs.

Although the above studies suggest that the distance between the radical and the chromophore may affect the efficiency of REISC, many other possible structural factors, for example conjugation length, radical type/number, electronic coupling, and geometrical influences, have not yet been taken into account. Lian et al. reported several analogous Bodipy-TEMPO derivatives **45–48**, in which TEMPO radicals were introduced into Bodipy chromophores through different lengths of the alkyl chain and different substitution positions (Fig. 43),[103] the authors studied the effect of the topology of the photosensitizer, i.e., the distance and the substitution position, on the promotion of the REISC efficiency.

The fluorescence quantum yield (Φ_F) of **45** is 99%, however, the fluorescence of the Bodipy-TEMPO was significantly quenched (Φ_F = 15%–19%) despite the long through-bond distance of 13 Å between Bodipy and TEMPO.[103] The triplet signals were observed in the fs- and ns-TA spectra of **46**, **47**, and **48**, suggesting that the free radicals indeed promote the ISC process. Interestingly, dyad **46** has the shortest through-bond distance, and it shows the fastest ISC rate (τ_{ISC} = 1.4 ns), but the longest triplet excited state lifetime (τ_T = 32 μs). To explain this anomalous phenomenon, the ground states spatial configurations of the dyads **45–48** were calculated by DFT (Fig. 44), and it was found that the shorter spatial distances of 3.59 Å and 2.48 Å, as result of folded geometry, it is probably responsible for the shorter triplet lifetimes of **47** and **48**, respectively. These results infer the geometry of the radical-chromophore also has a substantial effect on the ISC rate and triplet state yield, which is useful for designing the structure of PSs based on REISC mechanism.

We also achieved the regulation of triplet state by attaching a stable free radical to Bodipy dimers which show REISC mechanism (Fig. 45).[104] By incorporating two Bodipy units in the molecular structure, excited dimer is resulted upon photoexcitation, further altering the triplet excited state properties of Bodipy. Based on the previous studies on derivatization of the Bodipy, the reaction of *meso*-chloro-Bodipy with NH_2-TEMPO should directly introduce the TEMPO at the 8-position (**49**, Fig. 45), however, the isolated major product do not show the expected structure. Further analysis through ^{1}H NMR and single crystal X-ray diffraction (Fig. 46) revealed that under basic reaction conditions, a carbanion rearrangement occurred on the Bodipy aromatic ring, leading to the connection of the amino group to the 3- or 5-position methyl of Bodipy, rather than the structure expected

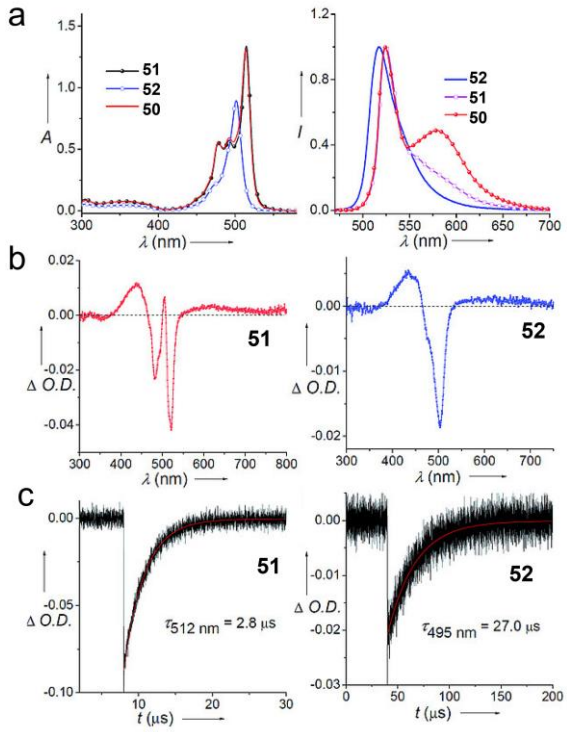

Fig. 47 (a) UV/Vis absorption spectra and normalized fluorescence emission spectra of **50**, **51**, and **52**, λ_{ex} = 460 nm in toluene. (b) The ns-TA difference spectra of **51** and **52** in deaerated toluene. λ_{ex} = 355 nm, (c) decay trance of triplet state of **51** and **52**. Reproduced with permission from ref. 104. Copyright 2018 Wiley-VCH.

according to the previously reported derivatization chemistry of Bodipy (compound **49**).[105,106]

In the steady-state UV/Vis absorption spectra (Fig. 47), compounds **50** and **51** both exhibit pronounced absorption bands centred at 514 nm, with two additional shoulders at 473 and 492 nm, which are different from the typical Bodipy chromophore absorption profile, indicates significant ground-state interactions between the Bodipy units in both **50** and **51.** It should be noted that the absorption profiles of **50** and **51** differ from those typical absorption character caused by exciton coupling, *J*- or *H*-aggregation in Bodipy chromophores, and they are also different from ground-state interactions seen in Bodipy dimers with co-facial geometries.[107,108] The unique UV/Vis spectra of **50** and **51** underscore the importance of the relative arrangement of the Bodipy units. Unlike C–C bonded Bodipy pairs at the 3,3′-positions, which show exciton coupling effects with split absorption bands,[109] **50** and **51** exhibit a novel absorption profile that was not observed in previous Bodipy derivatives, highlighting their specific intramolecular interaction.

The ns-TA spectrum of **52** is consistent with that of the conventional Bodipy (Fig. 47b), The triplet excited state absorption bands are centred at both 425 nm and 630 nm ($T_1 \rightarrow T_n$), the ground state bleaching (GSB) band is centred at 500 nm, the triplet state lifetime is 27 μs. The ns-TA spectra of **51** exhibit different triplet excited state properties compared to the monomeric **52**. Firstly, the GSB band shape of **51** differs from the steady-state absorption spectrum (three absorption peaks between 477 nm to 514 nm), a noticeable splitting appears in the ns-TA spectra with the disappearance of the GSB peak at 492 nm, this indicates the possibility of strong excited state absorption at 500 nm. Despite of the structural similarity between **51** and **52**, it can be inferred that, there is an interaction between the triplet state and the ground state in **51**, formation of a triplet excited dimer complex is likely. Additionally, the lifetime of triplet excited dimer complex is significantly shorter than that of the monomer, reflecting the intramolecular interaction between the two Bodipy groups. We used these Bodipy derivatives containing free radicals to TTA-UC, the strong upconversion luminescence was observed, with an upconversion quantum yield of 4.7%. This concept paved a new way for developing novel heavy atom-free triplet PSs to be used in TTA-UC, etc.

For the application of triplet PS in PDT, TTA-UC, and related areas, photosensitizers showing long wavelength absorption are desired. Thus, we designed a novel naphthalenediimide (NDI)-2,2,6,6-tetramethylpiperidinyloxy (TEMPO) dyad (compound **53**) with the absorption maximum at 606 nm,[71] the strong absorption of long wavelength is due to the amino substitution on the NDI chromophore (Fig. 48). With a TEMPO radical attached on the NDI chromophore, compound **53** may show the REISC ability to generate triplet state upon photoexcitation. The triplet state lifetime of the compound was determined as 8.7 μs. To determine the ISC rate constant, the fs-TA spectra of the compound was measured. The compound **53** exhibits a strong GSB band at 612 nm and significant positive absorption peaks between 400 nm – 590 nm (Fig. 49). With increasing of the delay time, the positive absorption peak at 570 nm evolved into a negative peak, thereby this peak is

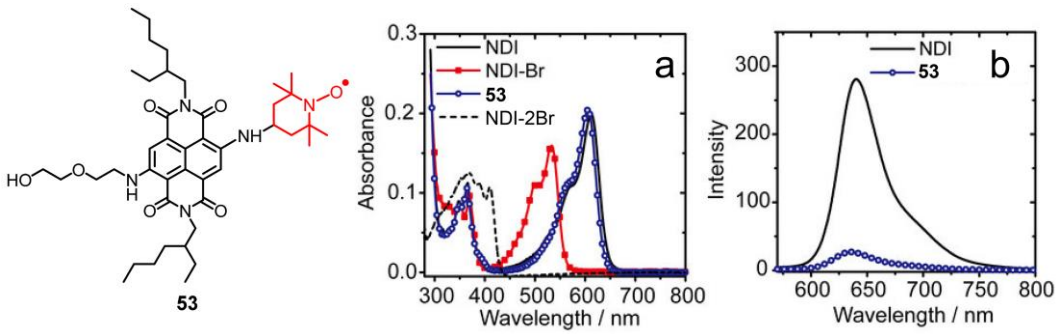

Fig. 48 Molecular structure of NDI-TEMPO dyad **53** and (a) UV/Vis absorption spectra of the compound **53** and reference compound, (b) fluorescence spectra of **53** is quenched compared with the reference compound NDI. Reproduced with permission from ref. 71. Copyright 2018 Wiley-VCH.

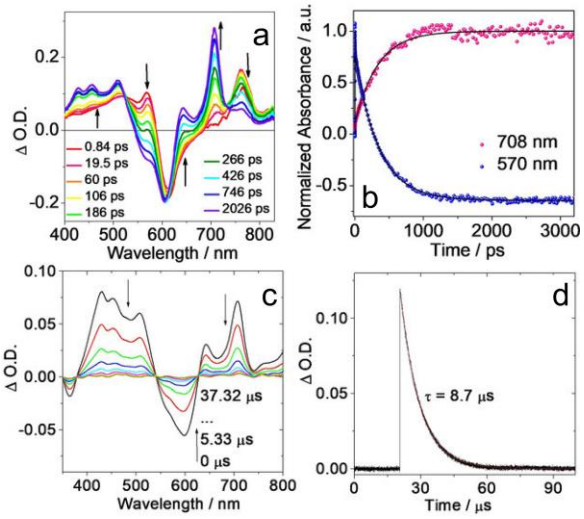

Fig. 49 (a) The fs-TA spectra of compound **53** and (b) decay trace at 708 and 570 nm, c = 2.5×10^{-4} M in toluene. (c) The ns-TA spectra of compound **53** and (b) decay trace at 430 nm, c = 5×10^{-6} M in toluene. Reproduced with permission from ref. 71. Copyright 2018 Wiley-VCH.

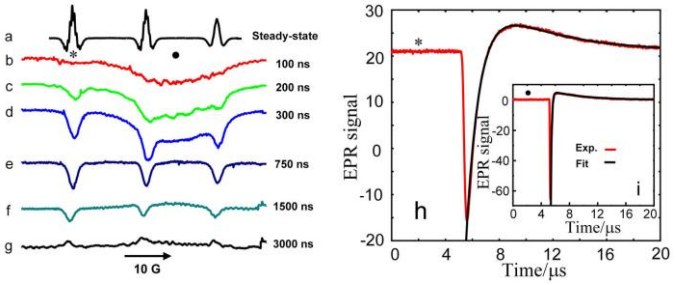

Fig. 50 (a) Steady state EPR spectrum of compound **53** in toluene at room temprature. (b–g) TREPR spectra of compound **53** in different delay times, and time evolution of EPR signals recorded at (h) * point and (i) • point in b–g. Reproduced with permission from ref. 71. Copyright 2018 Wiley-VCH.

attributed to the $S_1 \rightarrow S_n$ absorption band. A positive absorption peak appears at 700 nm at longer delay time, which is attributed to the $T_1 \rightarrow T_n$ absorption peak (which coincides with the peak position and shape in the ns-TA spectra). By fitting the kinetic decay at 708 nm, the ISC time constant of **53** was determined to be 338 ps (Fig. 49). The steady-state EPR spectrum of **53** exhibits three absorption peaks, which are characteristic signals of the TEMPO (Fig. 50). The TREPR spectrum of **53** was consisted of a broad peak and a set of three sharp peaks, the positions of these three sharp peaks are consistent with the signals of the TEMPO in the steady-state EPR spectrum, thus these bands are attributed to the spin-polarized ground state (D_0). Since the g value and the ^{14}N hyperfine coupling constant (a_N) value of the broad peak are larger than those of the D_0 state, thus the broad, structureless band is attributed to the excited state quartet Q (the broad peak represents the characteristic shape of the quartet state). The kinetic decay traces show that the spin polarization of both the D_0 state and the Q state change from emission-type (e) polarized signals to absorption-type (a) polarized signals (Fig. 50).

Because of the high triplet state quantum yield (Φ_T = 74%) of **53,** we used this novel triplet PS for TTA UC, the upconversion quantum yield was 2.6%. Since **53** has red-light region absorption (λ_{max} = 606 nm), efficient ISC ability and moderation triplet state lifetime (τ_1 = 8.7 μs), we also applied it for PDT (Fig. 51), when HeLa cells were incubated with different concentrations of **53** lipids for about 24 hours, the **53** lipids showed good phototoxicity after 14.4 J/cm^2 of 620 nm light irradiation. The EC50 (the concentration of photosensitiser that causes half the cells to die) was 3.22 μM (Fig. 51).

Perylenediimide (PBI) chromophore is one of the mostly investigated for its exceptional photophysical properties, include high photostability, high fluorescence quantum yield (close to 100%). However, it lacks the ISC ability to generate triplet state upon photoexcitation, therefore the study on PBI triplet state is limited. It was found that heavy atom effect cannot effectively promote the ISC of some PBI derivatives.[110] From the perspective of constructing triplet photosensitizer, we synthesized compound **54** which generates triplet state

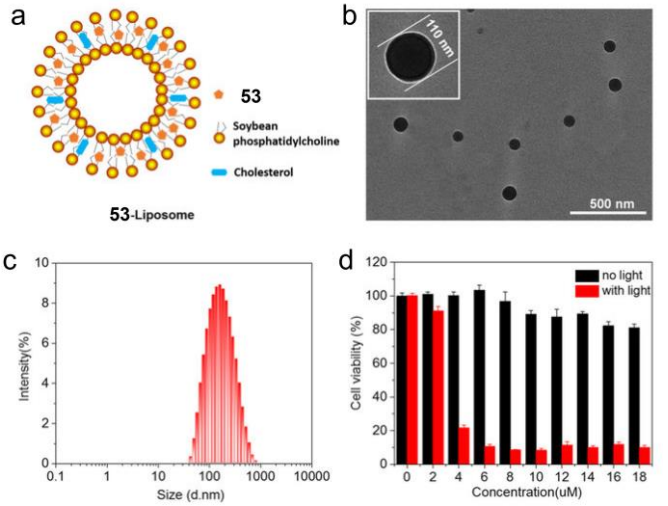

Fig. 51 (a) The structure and (b) TEM images of the **53**–liposome. (c) Particle size distribution measured by DLS. (d) Comparison of the cell viability of HeLa cells pretreated with increasing doses of **53**–liposome with and without light irradiation. Reproduced with permission from ref. 71. Copyright 2018 Wiley-VCH.

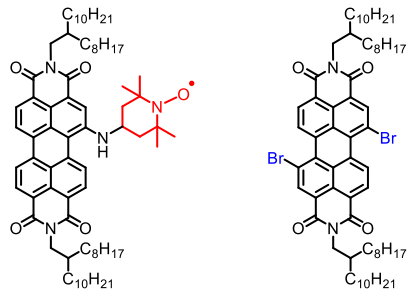

Fig. 52 Molecular structures of PBI-TEMPO compound **54** and reference compound **55**.

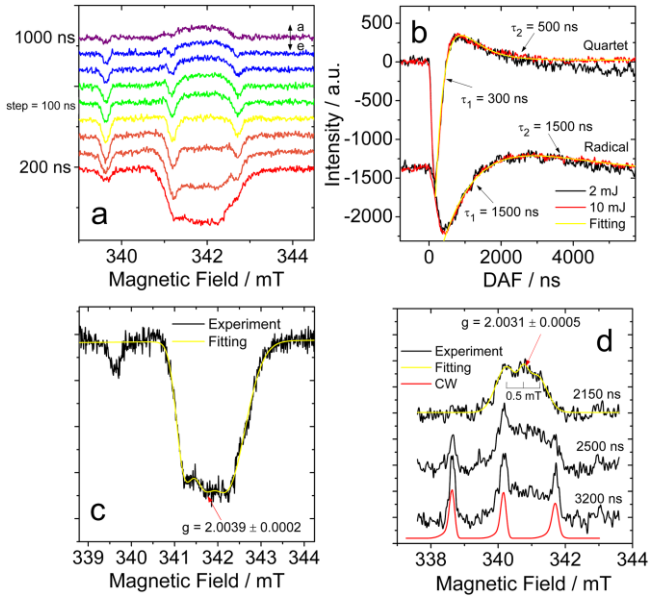

Fig. 53 (a) TREPR spectra of compound **54** recorded at X-band in toluene at room temperature, (b) decay trace of ground state (D_0 state at 339.6 mT) and Q state (341.8 mT) at different laser power of 2 mJ and 10 mJ. (c) TREPR spectra recorded at delay time of 200 ns after laser flash (yellow line is model emission spectrum with g = 2.0039 and a_Q = 0.5 mT) and (d) for 2150, 2500 and 3200 ns after laser flash (g = 2.0031 and a_Q = 0.5 mT). Reproduced with permission from ref. 110. Copyright 2021 Wiley-VCH.

through REISC mechanism, 4-amino-TEMPO was introduced to the bay position of PBI (Fig. 52).[110] The heavy atom effect is usually ineffective for PBI, and the ISC of **54** are more efficient than the control molecule with bromine atom substitution (compound **55**). For example, a new absorption band (607 nm, ε = 27000 M^{-1} cm^{-1}) was observed for **54** at the long wavelength because of the attached amino group, compound **54** have a higher singlet oxygen quantum yield (Φ_Δ = 32%, The Φ_Δ of **55** is only 18%) and the longer triplet lifetime (τ_T = 1.5 μs, τ_T of **55** is only 0.5 μs). We also studied the electron spin selectivity by TREPR spectra (Fig. 53), compound **54** is a strong exchange interaction system with the short linker, the TREPR spectra were record at X-band, the polarized Q excited state and D_0 state were observed (Fig. 53). The emission polarized signals at the initial time were transformed into enhanced absorption signals at longer delay time. The signal from the Q state show faster evolution than that from D_0 state, increasing the microwave frequency can increase the ESP inversion rate. The D_1 and Q states of **54** are mixed through ZFS effect, and electrons undergo a spin-selective transition of $D_1 \rightarrow Q$, and electrons preferentially populate on higher sub-levels (m_s = +3/2 and m_s = +1/2) of both states, thus generating the emission signal of Q state. At the same time, the spin-lattice relaxation makes the electrons populate on the lower sub-level (m_s = −3/2 and m_s = −1/2), resulting in the enhanced absorption signal of the Q state at longer delay time (Fig. 54). The population of D_1 states is induced by the difference of exchange interactions between D_2–D_1 (J_1) and D_1–D_0 (J_2), the REISC of compound **54** is explained by ΔJ-mechanism ($\Delta J = J_1 - J_2$).[111–113] We proposed that this molecular structure motif may become a general method for design of heavy atom-free triplet PSs.

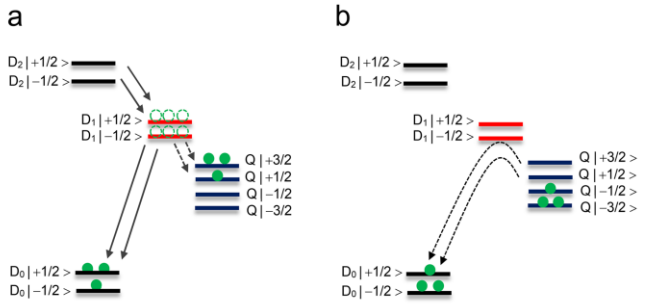

Fig. 54 ISC and polarization evolution mechanism of compound **54** at (a) early time populations and kinetics resulting in emissive polarization from D_1 and Q states followed by (b) enhanced absorption at later delay times. Reproduced with permission from ref. 110. Copyright 2021 Wiley-VCH.

5. Application of the triplet PSs based on REISC mechanism

There are already examples where REISC systems have been used as triplet PSs in in-vivo PDT studies. Song et al. prepared cyanine-TEMPO dyad as triplet PS and the application in PDT is promising (Fig. 55),[72] in which the TEMPO is attached at the *meso*-position of **56**, and the introduction of the radical resulted in a compound **57** showing an absorption peak at 660 nm and a fluorescence peak around 750 nm, with a large Stokes shift (100 nm). The reason is the intramolecular charge transfer process in the excited state between the 4-amino-TEMPO and dye **56**,[114,115] the introduction of TEMPO resulted in a significant increase in the singlet oxygen quantum yield of **56** from 0.6% to 20%. The ns-TA spectra study indicated a triplet state absorption of **57** at around 790 nm and a triplet state lifetime of about 9.16 μs. Before treatment with 100 % ICR mouse serum, **57** has a strong chemical stability, in addition, the dye has a low dark toxicity (IC50 value of 14.2 μM, Fig. 56).

Xu et al. utilized a similar approach by introducing TEMPO radical into the hemicyanine molecular structures (HCMDs) to prepare several radical-induced ISC-based photosensitizers, and investigated the photophysical processes of these photosensitizers as well as their applications in PDT in detail (Fig. 57).[116] The absorption and fluorescence spectra of **58** did not change significantly with introduction of TEMPO radical in the molecular structure, which were around 720 nm and 740 nm, respectively. Compared with control compound that has no TEMPO radical within the molecular structure (Φ_Δ=1.56%), the singlet oxygen quantum yields of **58** increased more than 20–fold (Φ_Δ = 32.3%), and the triplet state lifetime of **58** is 1.32 μs, which was very favourable for the PDT (Fig. 57).

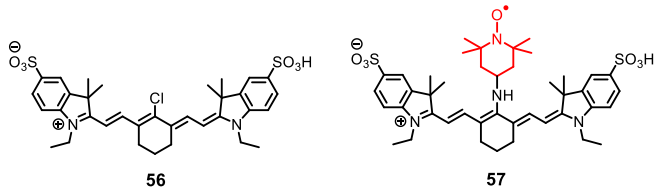

Fig. 55 Molecular structures of heptamethine cyanine **56** and compound **57** with TEMPO linked at the median position.

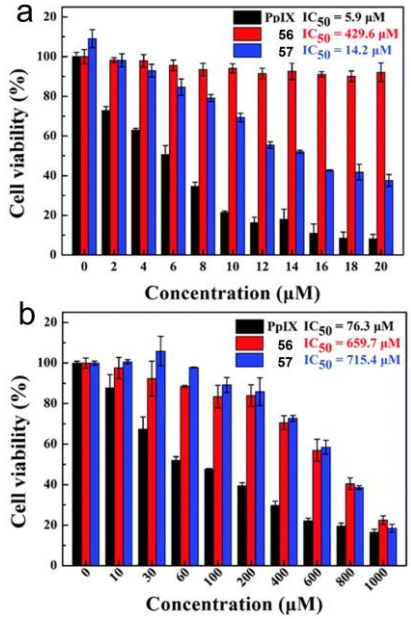

Fig. 56 (a) Phototoxicity evaluation and (b) dark cytotoxicity evaluation of dye **56** and dye **57** on HeLa cells after 20 min of irradiation, compared with a known PDT photosensitizer Protoporphyrin IX (PpIX), which has an excellent photocytotoxicity, λ_{ex} = 660 nm, 50 mW cm^{-2}. Reproduced with permission from ref. 72. Copyright 2018 Royal Society of Chemistry.

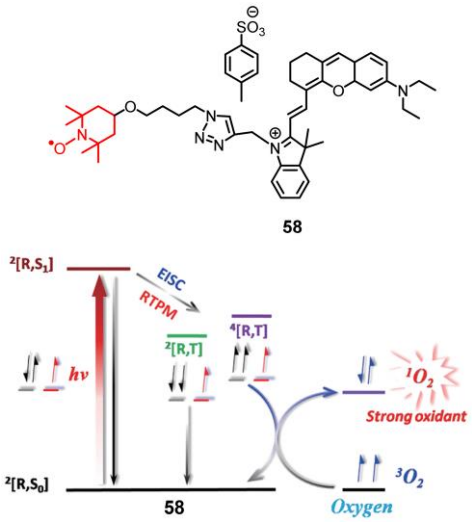

Fig. 57 Molecular structure of **58** and proposed mechanism to produce $^1O_2$. Reproduced with permission from ref. 116. Copyright 2021 Springer.

The TREPR spectra of **58** at room temperature showed a clear emission signal (*e* polarization) with three hyperfine lines centred at *g* = 2.0060, which corresponds to the polarized TEMPO with hyperfine coupling constant α_N = 1.65 mT.[117] The application of **58** in PDT showed that the compound has good cell permeability and is localized on mitochondria. Under the irradiation of 700 nm light, **58** could generate a large amount of ROS, disrupting the mitochondrial membrane potential and inducing apoptosis. Through the wrapping of PEG-SS-PCL micelles, **58** could be effectively delivered to tumours and inhibit tumour growth after PDT treatment (Fig. 58).

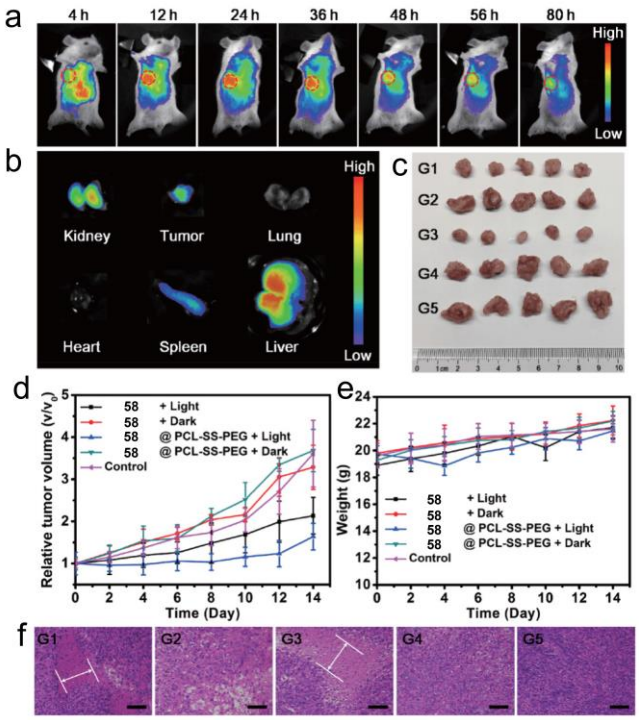

Fig. 58 (a) The vivo fluorescent imaging of 4T1 tumour bearing mice after the injection of **58**@PEG-SS-PCL nanoparticle at different time; (b) fluorescent imaging of different organs after 36 h intravenous injection of **58**@PEG-SS-PCL nanoparticle; (c) photo of tumour peeled from G1 to G5 after 14 d of PDT treatment; (d) relative tumour volume and (e) body weight of mice after different treatments; (f) H&E staining of tumour slice form each group. Scale bar: 100 μm (colour online). Reproduced with permission from ref. 116. Copyright 2021 Springer.

Yang et al. reported a stable π-radical dye **59** with near-infrared absorption (Fig. 59),[118] the compound can be used as a photosensitizer for TTA-UC, with appropriate acceptor, such as rubrene or perylene. Higher efficiency and larger anti-Stokes shift are widely pursued in study of TTA-UC system, NIR photosensitizers will increase the anti-Stokes shift to a certain extent, but it will also reduce the triplet state energy level and enhance the non-radiative transition of T_1 state, which is detrimental to TTA-UC. The strong electron-donating ability of TPA promote the formation of stable CS state, the CS absorption band was observed and extends absorption into the near infrared region (760 nm, $D_0 \rightarrow D_1$ transition), while maintaining a high energy level of D_1 state at 1.62 eV. This is beneficial to TTA-UC through subsequent doublet–triplet energy transfer produces the triplet state of acceptor. Because of the small energy gap between T_1 state of perylene and D_1 state of **59** (0.09 eV), reverse energy transfer from acceptors to **59** is possible (or inevitable), which may lead to decreased TTA-UC efficiency. This process of competition can be demonstrated by the delayed luminescence (τ_{DF} = 207 μs) of **59**, exactly two times of upconversion delays fluorescence lifetime (τ_{UC} = 99 μs). Nevertheless, the Φ_{UC} of the **59**–perylene system is still high up to 6.8%, at the same time the TTA-UC system show large anti-Stokes shift of 0.93 eV (Fig. 59). This work provides new ideas for designing heavy-atom-free triplet PSs with near infrared absorption.

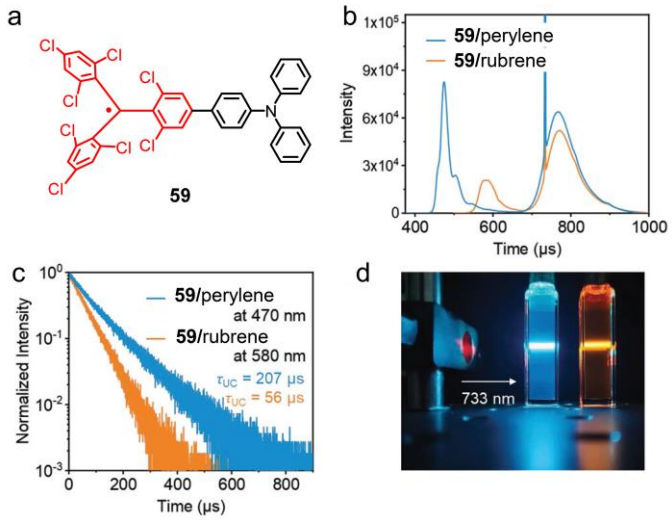

Fig. 59 (a) Molecular structure of π-radical dye **59** and (b) TTA-UC emission spectra of **59**/perylene and **59**/rubrene system under photoexcitation at of 733 nm, (c) time-resolved UC emission at 470 nm of **59**/perylene system and 580 nm of **59**/rubrene system, (d) photographs of TTA-UC fluorescence upon excitation with 733 nm laser. *c*[**59**] = 0.05 mM, *c*[perylene] = 8 mM, *c*[rubrene] = 15 mM, in toluene. Reproduced with permission from ref. 118. Copyright 2023 Wiley-VCH.

Recently, TEMPO radical was introduced to the molecular structure of a hemicyanine dye through flexible chain to obtain a REISC photosensitizer **60** (Fig. 60).[68] The dye has NIR absorption at about 668 nm, and a higher sensitization ability to produce singlet oxygen than the dye without TEMPO radical. The triplet state lifetime of **60** is about 1.25 μs, which is long enough to facilitate the energy transfer between the triplet excited state and molecular oxygen.

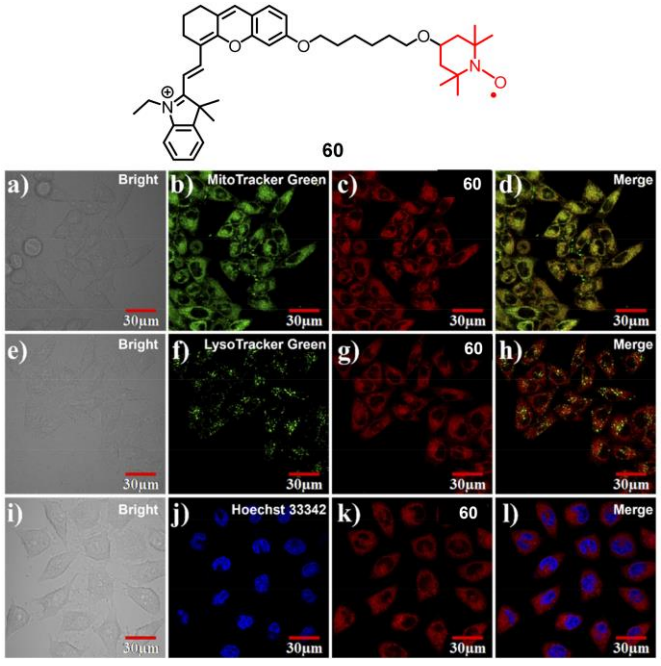

Fig. 60 Molecular structure of hemicyanine-TEMPO dye **60** with flexible chain and confocal images of **60** co-localize with (a-d) Mitotracker Green, (e-h) Lysotracker green and (i-l) Hoechst 33342 in MCF-7 cells. Reproduced with permission from ref. 68. Copyright 2024 Elsevier.

The authors use MitoTracker Green (a mitochondrial tracker), LysoTracker Green (a lysosome tracker), and Hoechst 33342 (a nuclear tracker) to study the permeability and distribution of **60** in MCF-7 cells (Fig. 60). The results showed that the compound **60** was clearly localized outside of the nucleus and had a better overlap with MitoTracker Green, suggesting that the **60** might mainly act on mitochondria to produce singlet oxygen (Fig. 60). In order to further investigate the potential application of compound in PDT, the phototoxicity and dark toxicity to cells were tested, Calcein-AM (AM) and propidium iodide (PI) were used (Fig. 61). The esterase in living cells can cut AM molecule to release green fluorescence, whereas PI can only permeable to the dead cells and combine with the double-stranded DNA to release red fluorescence. Using this method, MCF-7 cells were incubated with 5 μM **60** at 37 °C for 30 min, and treated with 660 nm light irradiation for 10 min and dark treatment, respectively. After further incubation and growth, the cells were stained with AM and PI and then imaging under LSCM. It was found that almost no cells died under dark conditions, suggests that the cytotoxicity of the **60** itself can be ignored. Under 660 nm light irradiation, the red channel was significantly increased and more dominant than the green channel, indicating that most cells died due to cytotoxicity caused by singlet oxygen produced triplet state. It is confirmed that compound **60** has a great application potential in PDT. In vivo studies of 4T1 tumour bearing mice model were also studied (Fig. 62). The excitation light 660 nm of **60** showed good tissue penetration ability in pork tissues of different thickness. 4T1 tumour was implanted subcutaneously into Balb/c mice and were treated with PBS, PBS + irradiation, **60** and **60** + irradiation, respectively. Only **60** and irradiation present at the same time, tumour growth was significantly inhibited, and there was no significant change in body weight of the mice during the treatment. Organs from four groups of mice were harvested and stained with hematoxylin

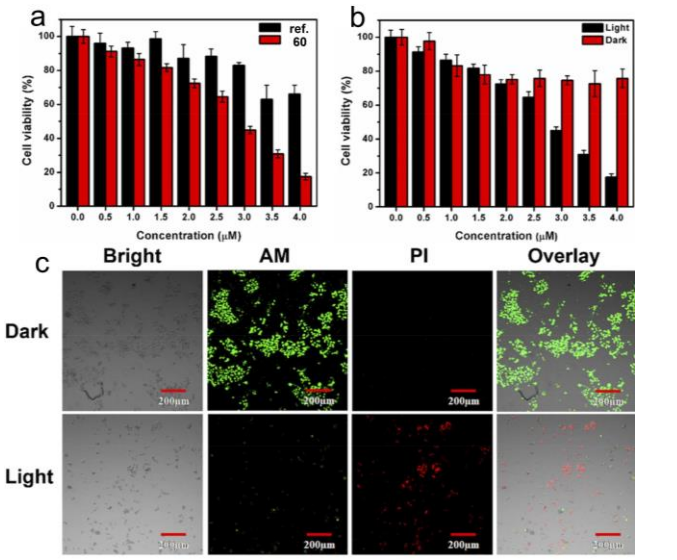

Fig. 61 (a) Cytotoxicity experiment of **60** and reference compound without radical at various concentrations irradiation for 10 min, λ_{ex} = 660 nm, (b) Cytotoxicity of **60** in the presence or absence of 660 nm light, (c) fluorescent imaging of Calcein-AM (AM) and Propidium iodide (PI) stained MCF-7 cells in the presence or absence of 660 nm light. Reproduced with permission from ref. 68. Copyright 2024 Elsevier.

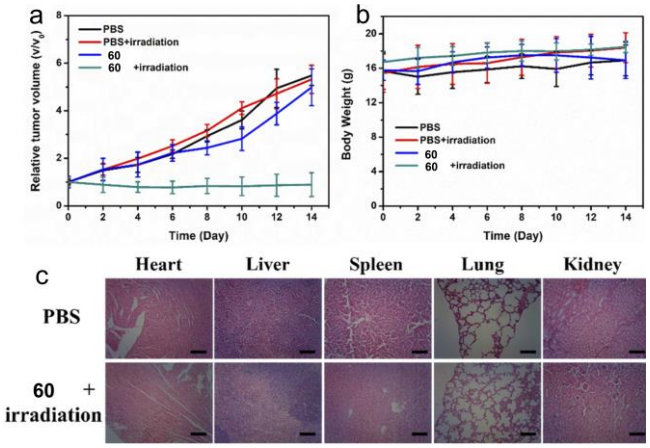

Fig. 62 (a) Relative tumor volume growth with different treatments, (b) body weight of mice in different groups during PDT process, (c) H&E stain of organ sections form PBS group and **60** + Light group after 14 days of treatments. Reproduced with permission from ref. 68. Copyright 2024 Elsevier.

and eosin (H&E), there are no histopathological or inflammatory lesions in each group. It was further confirmed that **60** constructed by REISC mechanism is an ideal photodynamic therapy reagent.

6. Conclusion and outlook

In summary, this review introduced the recent progress in free radical enhanced intersystem crossing (REISC), the production of high spin states (D and Q states), the mechanisms of electron spin polarization (ESP), as well as the molecular design methods. The applications of these novel triplet photosensitizers (PSs) in triplet-triplet annihilation upconversion (TTA-UC), photodynamic therapy (PDT), biological imaging are also discussed. We highlighted the importance of time-resolved electron paramagnetic resonance (TREPR) on study of the ESP properties and the high spin states (D and Q states). In particular, the potential application of REISC systems as qubits in quantum information science are promising. From the point of view of molecular design, there are a few methods available to control ESP pattern already, for example, using steric hindrance effect to restrict the conformation of radical and chromophore, or using different connection sites change the mutual orientation, and regulate the spin-orbit coupling of the states, etc. Although the REISC systems have developed for decades, there are many challenges in designing of triplet PSs based on this mechanism, such as the quenching effect of free radicals on the excited states of the chromophore, very often the molecules containing radical have short triplet lifetime, which is detrimental to the subsequent energy transfer process. Therefore, how to tune the molecular structure to optimize the triplet quantum yield and triplet lifetime simultaneously is still a challenge. The using of flexible linking groups, geometry regulation, and make the interaction in a suitable degree are the methods to address the above challenges. The reported examples are insufficient for deriving general rules, and it is necessary to further explore more molecular structure diversity. These studies will be useful for designing of new heavy atom-free triplet PSs.

Abbreviations

PBI	Perylenediimide
CR	Charge recombination
CS	Charge separation
ESP	Electron spin polarization
ESPT	Electron spin polarization transfer
fs-TA	Femtosecond transient absorption
HFI	Hyperfine coupling interaction
ISC	Intersystem crossing
LE	Locally excited state
LL'CT	Ligand to ligand electron transfer
ns-TA	Nanosecond transient absorption
PDT	Photodynamic therapy
PSs	Photosensitizers
REISC	Radical enhanced ISC
RP-ISC	Radical pair ISC
RQM	Reversed quartet mechanism
RQPM	Radical quartet pair mechanism
RTPM	Radical-triplet pair mechanism
SOC	Spin-orbital coupling
SOCMEs	Spin orbit coupling matrix elements
SOCT-ISC	Spin-orbital charge transfer ISC
TADF	Thermally activated delayed fluorescence
TREPR	Time resolved electron paramagnetic resonance
TTA-UC	Triplet-triplet annihilation up-conversion
ZFS	Zero field splitting

Author Contributions

X. Z. and J. Z. conceived the topic of the article. The initial manuscript was composed by X. Z., X. C., and Y. S., and revised by J. Z. The final version of the manuscript received approval from all authors.

Conflicts of interest

There are no conflicts to declare.

Acknowledgements

J. Zhao thanks the National Key Research and Development Program of China (2023YFE0197600), the NSFC (U2001222), the Fundamental Research Funds for the Central Universities (DUT22LAB610) for financial support. X. Zhang thanks Postdoctoral Fellowship Program of CPSF for financial support.

References

1. A. Rao, P. C. Y. Chow, S. Gélinas, C. W. Schlenker, C.-Z. Li, H.-L. Yip, A. K. Y. Jen, D. S. Ginger and R. H. Friend, *Nature*, 2013, **500**, 435–439.
2. C.-P. Lee, R. Y.-Y. Lin, L.-Y. Lin, C.-T. Li, T.-C. Chu, S.-S. Sun, J. T. Lin and K.-C. Ho, *RSC Adv.*, 2015, **5**, 23810–23825.
3. F. Etzold, I. A. Howard, N. Forler, A. Melnyk, D. Andrienko, M. R. Hansen and F. Laquai, *Energy Environ. Sci.*, 2015, **8**, 1511–1522.
4. G. N. Lim, C. O. Obondi and F. D'Souza, *Angew. Chem. Int. Ed.*, 2016, **55**, 11517–11521.
5. J. Ho, E. Kish, D. D. Méndez-Hernández, K. WongCarter, S. Pillai, G. Kodis, J. Niklas, O. G. Poluektov, D. Gust, T. A. Moore, A. L. Moore, V. S. Batista and B. Robert, *Proc. Natl. Acad. Sci.*, 2017, **114**, E5513–E5521.
6. D. R. Whang and D. H. Apaydin, *ChemPhotoChem*, 2018, **2**, 148–160.
7. Y. Cakmak, S. Kolemen, S. Duman, Y. Dede, Y. Dolen, B. Kilic, Z. Kostereli, L. T. Yildirim, A. L. Dogan, D. Guc and E. U. Akkaya, *Angew. Chem. Int. Edit.*, 2011, **50**, 11937–11941.
8. A. Kamkaew, S. H. Lim, H. B. Lee, L. V. Kiew, L. Y. Chung and K. Burgess, *Chem. Soc. Rev.*, 2013, **42**, 77–88.
9. V.-N. Nguyen, Y. Yan, J. Zhao and J. Yoon, *Acc. Chem. Res.*, 2021, **54**, 207–220.
10. T. N. Singh-Rachford and F. N. Castellano, *Coord. Chem. Rev.*, 2010, **254**, 2560–2573.
11. A. Monguzzi, R. Tubino, S. Hoseinkhani, M. Campione and F. Meinardi, *Phys. Chem. Chem. Phys.*, 2012, **14**, 4322–4332.
12. N. Yanai and N. Kimizuka, *Acc. Chem. Res.*, 2017, **50**, 2487–2495.
13. M. Montalti, A. Credi, L. Prodi and M. T. Gandolf, *Handbook of Photochemistry*, CRC Press, Boca Raton, 2006.
14. S. Amemori, Y. Sasaki, N. Yanai and N. Kimizuka, *J. Am. Chem. Soc.*, 2016, **138**, 8702–8705.
15. J. A. G. Williams, *Photochemistry and Photophysics of Coordination Compounds: Platinum*, Springer Berlin Heidelberg, Berlin, Heidelberg, 2007.
16. (*a*) L. Flamigni, A. Barbieri, C. Sabatini, B. Ventura and F. Barigelletti, *Photochemistry and Photophysics of Coordination Compounds: Iridium*, Springer Berlin Heidelberg, Berlin, Heidelberg, 2007; (*b*) Y. You and W. Nam, *Chem. Soc. Rev.*, 2012, **41**, 7061–7084.
17. S. Campagna, F. Puntoriero, F. Nastasi, G. Bergamini and V. Balzani, *Photochemistry and Photophysics of Coordination Compounds: Ruthenium*, Springer Berlin Heidelberg, Berlin, Heidelberg, 2007.
18. J. Karges, *Angew. Chem. Int. Ed.*, 2022, **61**, e202112236.
19. A. Gorman, J. Killoran, C. O'Shea, T. Kenna, W. M. Gallagher and D. F. O'Shea, *J. Am. Chem. Soc.*, 2004, **126**, 10619–10631.
20. T. Yogo, Y. Urano, Y. Ishitsuka, F. Maniwa and T. Nagano, *J. Am. Chem. Soc.*, 2005, **127**, 12162–12163.
21. X. Zhang, Z. Wang, Y. Hou, Y. Yan, J. Zhao and B. Dick, *J. Mater. Chem. C*, 2021, **9**, 11944–11973.
22. Y. Hou, X. Zhang, K. Chen, D. Liu, Z. Wang, Q. Liu, J. Zhao and A. Barbon, *J. Mater. Chem. C*, 2019, **7**, 12048–12074.
23. D. J. Gibbons, A. Farawar, P. Mazzella, S. Leroy-Lhez and R. M. Williams, *Photochem. Photobiol. Sci.*, 2020, **19**, 136–158.
24. J. W. Verhoeven, *J. Photochem. Photobiol. C: Photochem. Rev.*, 2006, **7**, 40–60.
25. T. Miura, R. Carmieli and M. R. Wasielewski, *J. Phys. Chem. A*, 2010, **114**, 5769–5778.
26. S. M. Harvey and M. R. Wasielewski, *J. Am. Chem. Soc.*, 2021, **143**, 15508–15529.
27. R. Carmieli, Q. Mi, A. B. Ricks, E. M. Giacobbe, S. M. Mickley and M. R. Wasielewski, *J. Am. Chem. Soc.*, 2009, **131**, 8372–8373.
28. T. Miura and M. R. Wasielewski, *J. Am. Chem. Soc.*, 2011, **133**, 2844–2847.
29. N. J. Turro, V. Ramamurthy and J. C. Scaiano, *Principles of Molecular Photochemistry: An Introduction*, University Science Books, Sausalito, CA, 2009.
30. M. T. Colvin, A. B. Ricks, A. M. Scott, D. T. Co and M. R. Wasielewski, *J. Phys. Chem. A*, 2012, **116**, 1923–1930.
31. H. van Willigen, G. Jones and M. S. Farahat, *J. Phys. Chem.*, 1996, **100**, 3312–3316.
32. Z. E. X. Dance, S. M. Mickley, T. M. Wilson, A. B. Ricks, A. M. Scott, M. A. Ratner and M. R. Wasielewski, *J. Phys. Chem. A*, 2008, **112**, 4194–4201.
33. M. A. Filatov, S. Karuthedath, P. M. Polestshuk, H. Savoie, K. J. Flanagan, C. Sy, E. Sitte, M. Telitchko, F. Laquai, R. W. Boyle and M. O. Senge, *J. Am. Chem. Soc.*, 2017, **139**, 6282–6285.
34. J. Zhao, K. Chen, Y. Hou, Y. Che, L. Liu and D. Jia, *Org. Biomol. Chem.*, 2018, **16**, 3692–3701.
35. G. Tang, A. A. Sukhanov, J. Zhao, W. Yang, Z. Wang, Q. Liu, V. K. Voronkova, M. Di Donato, D. Escudero and D. Jacquemin, *J. Phys. Chem. C*, 2019, **123**, 30171–30186.
36. K. Chen, I. V. Kurganskii, X. Zhang, A. Elmali, J. Zhao, A. Karatay and M. V. Fedin, *Chem. Eur. J.*, 2021, **27**, 7572–7587.
37. N. Rehmat, A. Toffoletti, Z. Mahmood, X. Zhang, J. Zhao and A. Barbon, *J. Mater. Chem. C*, 2020, **8**, 4701–4712.
38. N. Rehmat, I. V. Kurganskii, Z. Mahmood, Q. L. Guan, J. Zhao, Y. H. Xing, G. G. Gurzadyan and M. V. Fedin, *Chem. Eur. J.*, 2021, **27**, 5521–5535.
39. Y. Hou, I. Kurganskii, A. Elmali, H. Zhang, Y. Gao, L. Lv, J. Zhao, A. Karatay, L. Luo and M. Fedin, *J. Chem. Phys.*, 2020, **152**, 114701.
40. Z. Mahmood, M. Taddei, N. Rehmat, L. Bussotti, S. Doria, Q. Guan, S. Ji, J. Zhao, M. Di Donato, Y. Huo and Y. H. Xing, *J. Phys. Chem. C*, 2020, **124**, 5944–5957.
41. X. Zhao, A. A. Sukhanov, X. Jiang, J. Zhao and V. K. Voronkova, *J. Phys. Chem. Lett.*, 2022, **13**, 2533–2539.
42. X. Zhang, X. Liu, M. Taddei, L. Bussotti, I. Kurganskii, M. Li, X. Jiang, L. Xing, S. Ji, Y. Huo, J. Zhao, M. Di Donato, Y. Wan, Z. Zhao and M. V. Fedin, *Chem. Eur. J.*, 2022, **28**, e202200510.
43. X. Zhao and J. Zhao, *Chem. Commun.*, 2022, **58**, 7666-7669.
44. X. Zhang, X. Zhao, K. Ye and J. Zhao, *Chem. Eur. J.*, 2023, **29**, e202203737.
45. K. Schmidt, S. Brovelli, V. Coropceanu, D. Beljonne, J. Cornil, C. Bazzini, T. Caronna, R. Tubino, F. Meinardi, Z. Shuai and J.-L. Brédas, *J. Phys. Chem. A*, 2007, **111**, 10490–10499.
46. G. Orlandi and F. Negri, *Photochem. Photobiol. Sci.*, 2002, **1**, 289–308.
47. K. Nagarajan, A. R. Mallia, K. Muraleedharan and M. Hariharan, *Chem. Sci.*, 2017, **8**, 1776–1782.
48. Z. Wang, L. Huang, Y. Yan, A. M. El-Zohry, A. Toffoletti, J. Zhao, A. Barbon, B. Dick, O. F. Mohammed and G. Han, *Angew. Chem. Int. Ed.*, 2020, **59**, 16114–16121.
49. Y. Yan, A. A. Sukhanov, M. H. E. Bousquet, Q. Guan, J. Zhao, V. K. Voronkova, D. Escudero, A. Barbon, Y. Xing, G. G. Gurzadyan and D. Jacquemin, *J. Phys. Chem. B*, 2021, **125**, 6280–6295.
50. X. Zhang, A. A. Sukhanov, X. Liu, M. Taddei, J. Zhao, A. Harriman, V. K. Voronkova, Y. Wan, B. Dick and M. Di Donato, *Chem. Sci.*, 2023, **14**, 5014–5027.
51. K. Ishii, Y. Hirose, H. Fujitsuka, O. Ito and N. Kobayashi, *J. Am. Chem. Soc.*, 2001, **123**, 702–708.
52. E. M. Giacobbe, Q. Mi, M. T. Colvin, B. Cohen, C. Ramanan, A. M. Scott, S. Yeganeh, T. J. Marks, M. A. Ratner and M. R. Wasielewski, *J. Am. Chem. Soc.*, 2009, **131**, 3700–3712.
53. S. Weber, *eMagRes*, 2017, **6**, 255–270.
54. B. K. Rugg, M. D. Krzyaniak, B. T. Phelan, M. A. Ratner, R. M. Young and M. R. Wasielewski, *Nat. Chem.*, 2019, **11**, 981–986.
55. M. Mayländer, O. Nolden, M. Franz, S. Chen, L. Bancroft, Y. Qiu, M. R. Wasielewski, P. Gilch and S. Richert, *Chem. Sci.*, 2022, **13**, 6732–6743.

56. M. Mayländer, T. Quintes, M. Franz, X. Allonas, A. Vargas Jentzsch and S. Richert, *Chem. Sci.*, 2023, **14**, 5361–5368.
57. Y. Qiu, H. J. Eckvahl, A. Equbal, M. D. Krzyaniak and M. R. Wasielewski, *J. Am. Chem. Soc.*, 2023, **145**, 25903–25909.
58. K. Kopp, L. Westhofen, T. Hett, M. Felix Schwering-Sohnrey, M. Mayländer, S. Richert and O. Schiemann, *Chem. Eur. J.*, 2024, **30**, e202303635.
59. J.-i. Fujisawa, K. Ishii, Y. Ohba, S. Yamauchi, M. Fuhs and K. Möbius, *J. Phys. Chem. A*, 1999, **103**, 213–216.
60. J.-i. Fujisawa, K. Ishii, Y. Ohba, S. Yamauchi, M. Fuhs and K. Möbius, *J. Phys. Chem. A*, 1997, **101**, 5869–5876.
61. A. I. Shushin, *J. Phys. Chem. A*, 2014, **118**, 11355–11363.
62. A. Blank and H. Levanon, *J. Phys. Chem. A*, 2001, **105**, 4799–4807.
63. J.-i. Fujisawa, K. Ishii, Y. Ohba, M. Iwaizumi and S. Yamauchi, *J. Phys. Chem.*, 1995, **99**, 17082–17084.
64. M. T. Colvin, E. M. Giacobbe, B. Cohen, T. Miura, A. M. Scott and M. R. Wasielewski, *J. Phys. Chem. A*, 2010, **114**, 1741–1748.
65. M. L. Kirk, D. A. Shultz, J. Chen, P. Hewitt, D. Daley, S. Paudel and A. van der Est, *J. Am. Chem. Soc.*, 2021, **143**, 10519–10523.
66. M. L. Kirk, D. A. Shultz, P. Hewitt and A. van der Est, *J. Phys. Chem. Lett.*, 2022, **13**, 872–878.
67. M. L. Kirk, D. A. Shultz, P. Hewitt, D. E. Stasiw, J. Chen and A. van der Est, *Chem. Sci.*, 2021, **12**, 13704–13710.
68. F. Xu, Y. Zhang, D. Lai, Y. Yang, J. Cai, C. Tang, C. Zhou, D. Cen, G. Xiang and X. Zheng, *Sensor Actuat. B-Chem*, 2024, **401**, 134955.
69. X. Cui, Z. Zhang, Y. Yang, S. Li and C.-S. Lee, *Explor.*, 2022, **2**, 20210264.
70. Z. Wang, J. Zhao, A. Barbon, A. Toffoletti, Y. Liu, Y. An, L. Xu, A. Karatay, H. G. Yaglioglu, E. A. Yildiz and M. Hayvali, *J. Am. Chem. Soc.*, 2017, **139**, 7831–7842.
71. Z. Wang, Y. Gao, M. Hussain, S. Kundu, V. Rane, M. Hayvali, E. A. Yildiz, J. Zhao, H. G. Yaglioglu, R. Das, L. Luo and J. Li, *Chem. Eur. J.*, 2018, **24**, 18663–18675.
72. L. Jiao, F. Song, J. Cui and X. Peng, *Chem. Commun.*, 2018, **54**, 9198–9201.
73. C. Corvaja, M. Maggini, M. Prato, G. Scorrano and M. Venzin, *J. Am. Chem. Soc.*, 1995, **117**, 8857–8858.
74. J.-i. Fujisawa, Y. Ohba and S. Yamauchi, *J. Phys. Chem. A*, 1997, **101**, 434–439.
75. J. W. Arbogast, A. P. Darmanyan, C. S. Foote, F. N. Diederich, R. L. Whetten, Y. Rubin, M. M. Alvarez and S. J. Anz, *J. Phys. Chem.*, 1991, **95**, 11–12.
76. H. Levanon and J. R. Norris, *Chem. Rev.*, 1978, **78**, 185-198.
77. H. Levanon, *Rev. Chem. Intermed.*, 1987, **8**, 287–320.
78. H. Levanon, A. Regev, T. Galili, M. Hugerat, C. K. Chang and J. Fajer, *J. Phys. Chem.*, 1993, **97**, 13198–13205.
79. K. Ishii, Y. Hirose and N. Kobayashi, *J. Phys. Chem. A*, 1999, **103**, 1986–1990.
80. K. Ishii, *Coordin. Chem. Rev.*, 2012, **256**, 1556–1568.
81. X.-J. Jiang, P.-C. Lo, S.-L. Yeung, W.-P. Fong and D. K. P. Ng, *Chem. Commun.*, 2010, **46**, 3188–3190.
82. Y. Teki, H. Tamekuni, K. Haruta, J. Takeuchi and Y. Miura, *J. Mater. Chem.*, 2008, **18**, 381–391.
83. Y. Teki, H. Tamekuni, J. Takeuchi and Y. Miura, *Angew. Chem. Int. Ed.*, 2006, **45**, 4666–4670.
84. S. Richert, C. E. Tait and C. R. Timmel, *J. Magn. Reson.*, 2017, **280**, 103–116.
85. X. Xiao, K. Ye, M. Imran and J. Zhao, *Appl. Sci.*, 2022, ***12***, 9933.
86. S. M. Dyar, E. A. Margulies, N. E. Horwitz, K. E. Brown, M. D. Krzyaniak and M. R. Wasielewski, *J. Phys. Chem. B*, 2015, **119**, 13560–13569.
87. P. K. Poddutoori, Y. E. Kandrashkin, P. Karr and A. van der Est, *J. Chem. Phys.*, 2019, **151**, 204303.
88. C. Godfrin, A. Ferhat, R. Ballou, S. Klyatskaya, M. Ruben, W. Wernsdorfer and F. Balestro, *Phys. Rev. Lett.*, 2017, **119**, 187702.
89. K. E. Smyser and J. D. Eaves, *Sci. Rep.*, 2020, **10**, 18480.
90. M. T. Colvin, R. Carmieli, T. Miura, S. Richert, D. M. Gardner, A. L. Smeigh, S. M. Dyar, S. M. Conron, M. A. Ratner and M. R. Wasielewski, *J. Phys. Chem. A*, 2013, **117**, 5314–5325.
91. E. T. Chernick, R. Casillas, J. Zirzlmeier, D. M. Gardner, M. Gruber, H. Kropp, K. Meyer, M. R. Wasielewski, D. M. Guldi and R. R. Tykwinski, *J. Am. Chem. Soc.*, 2015, **137**, 857–863.
92. M. L. Kirk, D. A. Shultz, P. Hewitt, J. Chen and A. van der Est, *J. Am. Chem. Soc.*, 2022, **144**, 12781–12788.
93. Y. Huang, Z. Xu, S. Jin, C. Li, K. Warncke, F. A. Evangelista, T. Lian and E. Egap, *Chem. Mater.*, 2018, **30**, 7840–7851.
94. O. Nolden, N. Fleck, E. R. Lorenzo, M. R. Wasielewski, O. Schiemann, P. Gilch and S. Richert, *Chem. Eur. J.*, 2021, **27**, 2683–2691.
95. T. Lazarides, T. M. McCormick, K. C. Wilson, S. Lee, D. W. McCamant and R. Eisenberg, *J. Am. Chem. Soc.*, 2011, **133**, 350–364.
96. R. P. Sabatini, B. Zheng, W.-F. Fu, D. J. Mark, M. F. Mark, E. A. Hillenbrand, R. Eisenberg and D. W. McCamant, *J. Phys. Chem. A*, 2014, **118**, 10663–10672.
97. A. Ito, N. Kobayashi and Y. Teki, *Inorg. Chem.*, 2017, **56**, 3794–3808.
98. W. Yang, A. A. Sukhanov, J. H. Lim, X. Li, Y. Meng, J. Zhao, H. Sun, J. Y. Lee, G. G. Gurzadyan and V. K. Voronkova, *Inorg. Chem.*, 2020, **59**, 12471–12485.
99. K. Nishimura, R. Yabuki, T. Hamachi, N. Kimizuka, K. Tateishi, T. Uesaka and N. Yanai, *J. Phys. Chem. B*, 2023, **127**, 1219–1228.
100. V. Rane and R. Das, *J. Phys. Chem. A*, 2015, **119**, 5515–5523.
101. V. Rane and R. Das, *J. Phys. Chem. A*, 2014, **118**, 8689–8694.
102. R. N. Schwartz, L. L. Jones and M. K. Bowman, *J. Phys. Chem.*, 1979, **83**, 3429–3434.
103. Z. Xu, Y. Huang, Y. Cao, T. Jin, K. A. Miller, A. L. Kaledin, D. G. Musaev, T. Lian and E. Egap, *J. Chem. Phys.*, 2020, **153**, 154201.
104. K. Xu, A. A. Sukhanov, Y. Zhao, J. Zhao, W. Ji, X. Peng, D. Escudero, D. Jacquemin and V. K. Voronkova, *Eur. J. Org. Chem.*, 2018, **7**, 885–895.
105. Z. Mahmood and J. Zhao, *Photochem. Photobiol. Sci.*, 2016, **15**, 1358–1365.
106. L. Wang, J.-W. Wang, A.-j. Cui, X.-X. Cai, Y. Wan, Q. Chen, M.-Y. He and W. Zhang, *RSC Adv.*, 2013, **3**, 9219–9222.
107. Y. Tokoro, A. Nagai and Y. Chujo, *Tetrahedron Lett.*, 2010, **51**, 3451–3454.
108. S. Choi, J. Bouffard and Y. Kim, *Chem. Sci.*, 2014, **5**, 751–755.
109. M. Bröring, R. Krüger, S. Link, C. Kleeberg, S. Köhler, X. Xie, B. Ventura and L. Flamigni, *Chem. Eur. J.*, 2008, **14**, 2976–2983.
110. X. Zhang, A. A. Sukhanov, E. A. Yildiz, Y. E. Kandrashkin, J. Zhao, H. G. Yaglioglu and V. K. Voronkova, *ChemPhysChem*, 2021, **22**, 55–68.
111. D. F. Evans, *J. Chem. Soc.*, 1957, 3885–3888.
112. Y. Kandrashkin and A. van der Est, *J. Chem. Phys.*, 2004, **120**, 4790–4799.
113. Y. E. Kandrashkin and A. van der Est, *J. Chem. Phys.*, 2019, **151**, 184301.
114. F. Song, X. Peng, E. Lu, R. Zhang, X. Chen and B. Song, *J. Photoch. Photobio., A: Chem*, 2004, **168**, 53–57.
115. X. Peng, F. Song, E. Lu, Y. Wang, W. Zhou, J. Fan and Y. Gao, *J. Am. Chem. Soc.*, 2005, **127**, 4170–4171.
116. F. Xu, H. Ge, N. Xu, C. Yang, Q. Yao, S. Long, W. Sun, J. Fan, X. Xu and X. Peng, *Sci. China. Chem.*, 2021, **64**, 488–498.
117. D. Swain, A. Rana, P. K. Panda and S. Venugopal Rao, *Chem. Phys. Lett.*, 2014, **610-611**, 310–315.
118. Y. Wei, K. An, X. Xu, Z. Ye, X. Yin, X. Cao and C. Yang, *Adv. Opt. Mater.*, 2024, **12**, 2301134.